We are IntechOpen, the world's leading publisher of Open Access books Built by scientists, for scientists

4,800
Open access books available

122,000
International authors and editors

135M
Downloads

154
Countries delivered to

Our authors are among the

TOP 1%
most cited scientists

12.2%
Contributors from top 500 universities

CLARIVATE ANALYTICS
BOOK CITATION INDEX
INDEXED

WEB OF SCIENCE™

Selection of our books indexed in the Book Citation Index
in Web of Science™ Core Collection (BKCI)

Interested in publishing with us?
Contact book.department@intechopen.com

FMR Studies of [SnO$_2$/Cu-Zn Ferrite] Multilayers

R. Singh and S. Saipriya

Additional information is available at the end of the chapter

http://dx.doi.org/10.5772/56330

1. Introduction

The artificially structured multilayers (ML) have opened a new field of interface magnetism. It is possible to fabricate a multilayer sample with a specific design according to the requirement consisting of magnetic, non-magnetic, metallic or non-metallic components. Various types of interfaces may be synthesized in ML by combining a magnetic component with a non-magnetic one or from two different magnetic components. The interface between two non-magnetic components is particularly interesting if a magnetic anomaly happens to be induced at the interface atom layer due to some interface effect.

The oscillations of magnetic parameters as a function of the number of interfaces, spacer layer or magnetic layer thickness in the ML have been gaining attention in the recent years. Bruno et al [1] employed RKKY model and Edwards et al [2] used spin dependent confinement of electrons in the quantum well provided by the spacer layer (quantum interference) to explain the oscillations initially observed in metallic ML. Exchange coupling in ML is also affected by direct dipolar coupling like the correlation of spins at rough interfaces (orange peel coupling), which is magnetostatic in origin and occurs due to the interaction of the dipoles which appear due to the roughness of the material [3]. This coupling favors parallel or anti-parallel alignment of spins depending upon the interplay between the magnetostatic exchange and anisotropy energy.

The oscillations in exchange coupling are also observed in oxide ML apart from the metallic ML [4]. Oxide materials are more stable and their ML can form magnetic structures which do not exist in bulk form. There are reports on ML of ferrites used along with NiO [5,6], MgO [7] , CoO [8] and SnO$_2$ [9-12].

The mixed spinel structure of Cu-Zn ferrites with composition $Cu_{0.6}Zn_{0.4}Fe_3O_4$ (CZF) gives high magnetization when deposited in Ar environment [13]. The properties of non-magnetic (NM) SnO$_2$ are sensitive to oxygen vacancies [14]. The interfacial region between these two materials may give rise to interesting magnetic phenomena. The objective of the present

work is to study the magnetic properties of SnO_2 and Cu-Zn Ferrite multilayers and interpret them in terms of suitable magnetization mechanism.

This chapter is about the Ferromagnetic Resonance (FMR) studies of (SnO_2/Cu-Zn Ferrrite) ML as a function of CZF layer thickness and SnO_2 layer thickness.

2. Experimental

Alternate layers of SnO_2 and $Cu_{0.6}Zn_{0.4}Fe_3O_4$ (CZF) were deposited on quartz substrates at room temperature (RT) using rf-magnetron sputtering in Ar environment from SnO_2 and CZF targets at a power of 50W and 70W respectively. The rate of deposition was estimated by depositing thin films of SnO_2 and CZF separately. The synthesis method of targets and the rf sputtering system are described in our earlier work [15]. The field emission scanning electron microscopy (FESEM) studies were carried out to observe the multilayer structure. The FMR studies were carried out in the temperature range 100 - 450 K using JEOL x-band spectrometer. FMR studies were carried out at different temperatures and by varying the angle θ_H between the thin film normal and the direction of the applied field. The peak-to-peak FMR signal intensity (I_{PP}) which is proportional to the power absorbed was measured between the positive and negative peak points along the y-axis. The peak-to-peak linewidth (ΔH) was measured as a function of temperature.

3. Ferromagnetic Resonance (FMR) studies

3.1. Effect of CZF layer thickness

The ML samples [SnO_2 (46 nm)/CFZ(x nm)]$_5$ where x = 42 nm, 83 nm and 249 nm were synthesized. A final capping layer of 46 nm of SnO_2 was deposited on all the ML samples. The error in the thickness is ± 5 nm. The FESEM images (figure 1) portray a stack of alternate dark and light layers corresponding to CZF and SnO_2 respectively as confirmed by the EDAX data. The CZF layer exhibits a columnar growth as observed in many of the sputtered films [16]. The protrusions of CZF column into SnO_2 layers visible from the FESEM images indicate that the interfaces are diffused.

FMR studies were carried out at different temperatures and by varying the angle θ_H between the thin film normal and the direction of the applied field. Figure 2 shows the room temperature FMR spectra of the ML in θ_H = 90° (parallel) and 0° (perpendicular) configuration. In the parallel geometry, the FMR signal for the ML with x = 249 nm is highly asymmetric. The steep increase in the low field side and a slow increase in the high field side indicate negative anisotropy in the ML [17].

The line shape of FMR signal is sensitive to magnetic interactions in the material and hence a change in line shape is an indication of change in the magnetic interactions in the ML. Many a times the observed single FMR signal may arise from overlapping of 2 or more FMR signals.
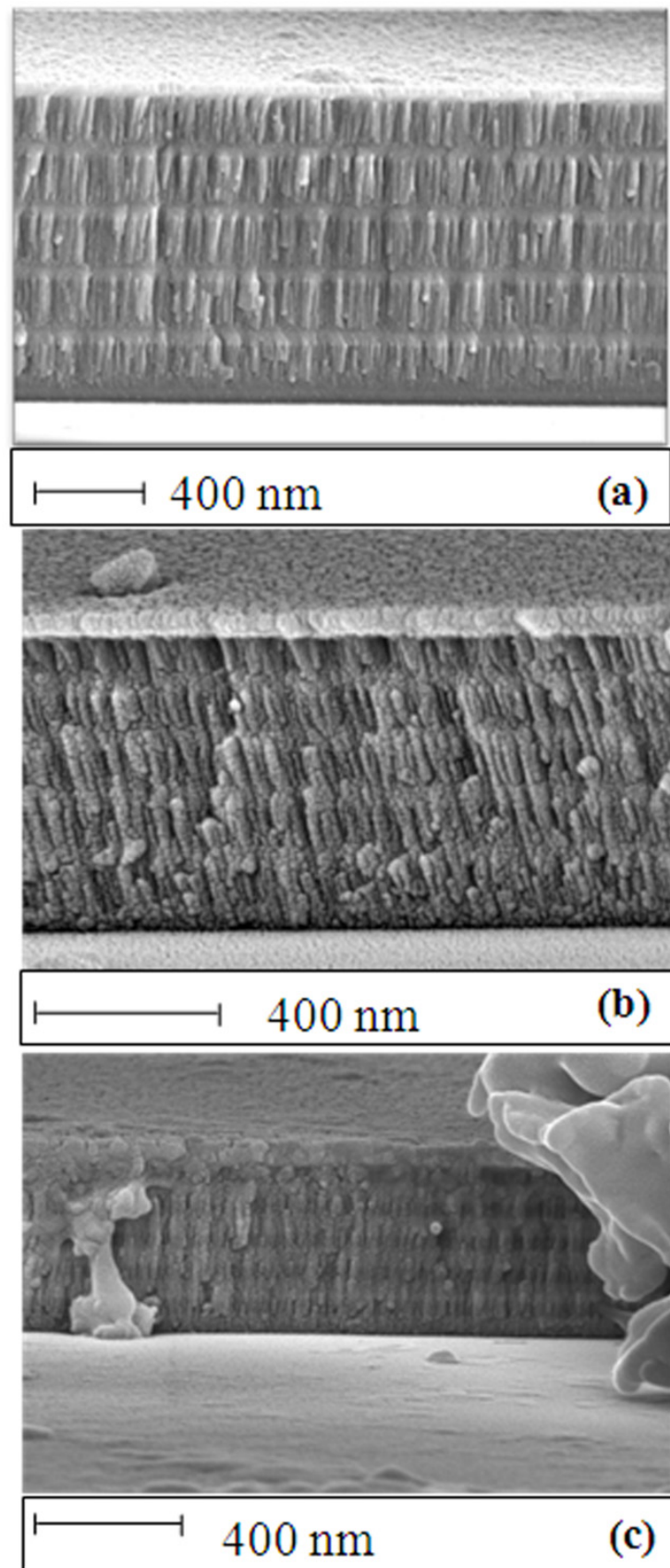
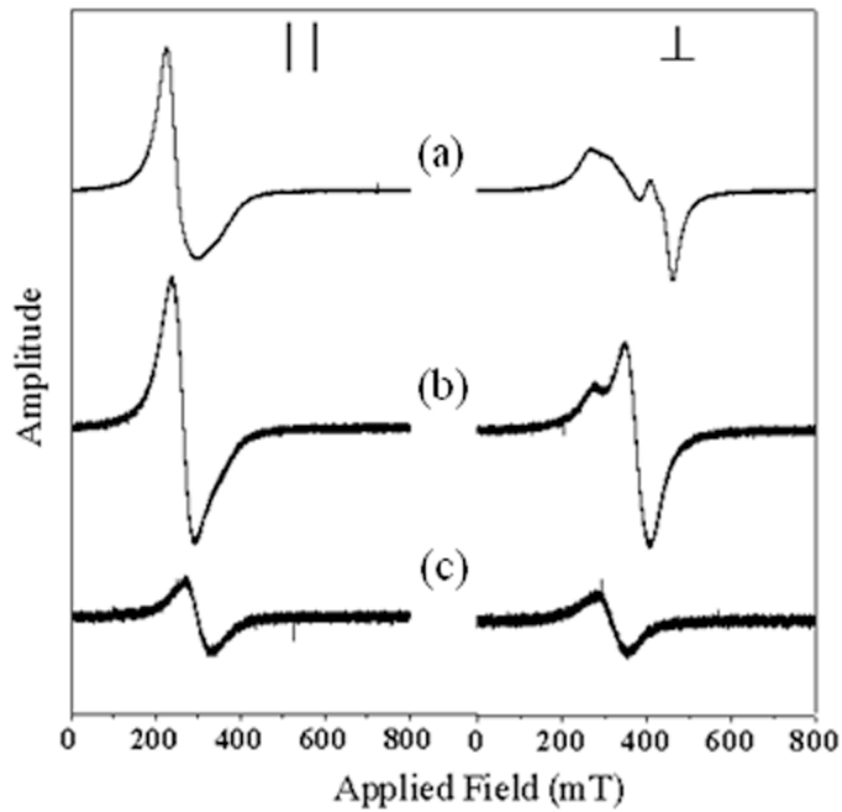**Figure 1.** FESEM images of [SnO$_2$ (46nm) CZF (x nm)]$_5$ for x = 249 (a), 83(b) and 42 nm (c).

Figure 2. RT FMR spectra of [SnO$_2$ (46 nm) CZF(x nm)]$_5$ in the parallel and perpendicular configuration for x = 249 (a), 83(b) and 42 nm (c).
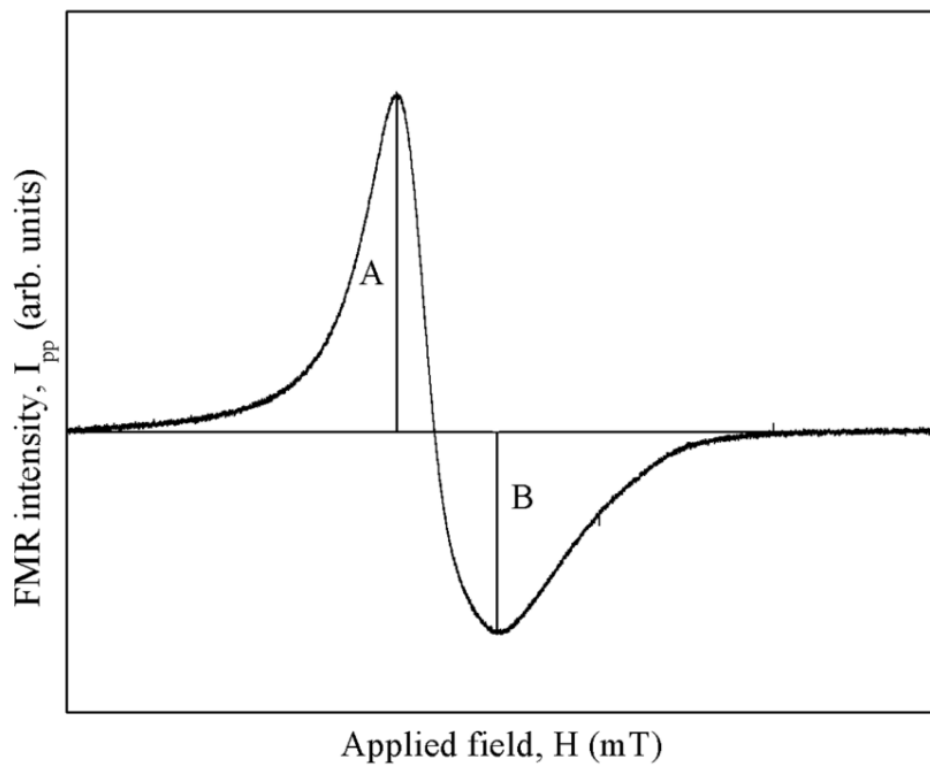

Figure 3. A representative FMR plot depicting the A/B ratio.

The asymmetry parameter, A/B ratio, was estimated by dividing the intensity of the upper part of the FMR signal by that of the lower part (figure 3). A/B > 1 indicates that the intensity of the upper half of the FMR signal is higher than the lower one and vice versa. A/B = 1 indicates a signal with both its upper and lower half with equal intensity.

The A/B ratio at room temperature in the parallel configuration is 1.27, 1.12 and 0.69 for x = 249, 83 and 42 nm respectively. A/B > 1 gives Dysonian line shape to the spectrum which results from lower skin depth and higher conductivity of the sample [18]. Hence the possibility of occurrence of dispersive component due to diffusion of electrons into and out of the skin region cannot be ruled out for the ML with x = 249 and 83 nm.

The asymmetric nature of the FMR spectra of x = 249 nm may also be attributed to the interlayer coupling in the ML. The asymmetry decreases with decrease in CFZ layer thickness presumably due to the decrease in the interlayer coupling strength between the layers. As a consequence of interlayer coupling, the coupled spins precess out of phase with the uncoupled ones. Hence the FMR spectra of spins which precess at different frequencies overlap to give an asymmetric signal [19]. The peak to peak FMR signal intensity (I_{PP}) is measured between the positive and negative peak points along the y-axis and is proportional to the power absorbed. In the parallel configuration I_{PP} values, normalized to the volume of the CZF layers, increases as the magnetic layer (CZF) thickness increases from x = 42 to 83 nm followed by a decrease for x = 249 nm. The resonance field (H_{res}) decreases with increase in the CFZ layer thickness in this geometry. This is attributed to the increase in internal field with increasing CZF layer (magnetic layer) thickness because of which the magnetization also increases. The FMR parameters for both parallel and perpendicular configuration are listed in table 1.

The intrinsic line shape and linewidth of an FMR signal is sensitive to variation of magnetization at the interfaces, surface pits, grain boundaries etc. The peak to peak linewidth (ΔH) is sensitive to inhomogeneity, surface roughness, internal field etc. ΔH values for the ML reported in this study initially decreases from 631 to 541 Oe as x changes from 42 to 83 nm followed by an increase to 704 Oe for x = 249 nm. The ratio of the active layer thickness to dead layer thickness is low for ML with x = 42 nm. As x changes from 42 to 83 nm, the contribution from the dead layer becomes relatively negligible due to large active layer thickness. The increase in ΔH for x = 249 nm may be due to the presence of interlayer coupling [20].

The ML with x = 249 nm exhibits multiple resonances in θ_H = 0° configuration at RT (figure 2). The resonances occur at 363 and 418 mT for this ML. The occurrence of multiple resonances may be attributed to the excitation of spin waves due to the inter layer coupling of CZF layers mediated by the non-magnetic SnO₂ layers [21]. This implies that the entire ML is coupled by the interlayer exchange coupling as a single magnetic entity. The spin waves propagate through the SnO₂ layers and are sustained by the entire multilayer film. This confirms that for x = 249 nm the CZF layer thickness is ample enough to polarize SnO₂ layer. With decreasing x it loses its capacity to polarize SnO₂ layer. The occurrence of

multiple resonances may also be attributed to the existence of two different magnetic phases pertaining to the interfacial region and the bulk of the magnetic layer.

The number of resonances decreases with decreasing CZF thickness in the perpendicular geometry. As the thickness of CZF layer increases, the ML provides sufficient length for the spin wave modes to be formed.
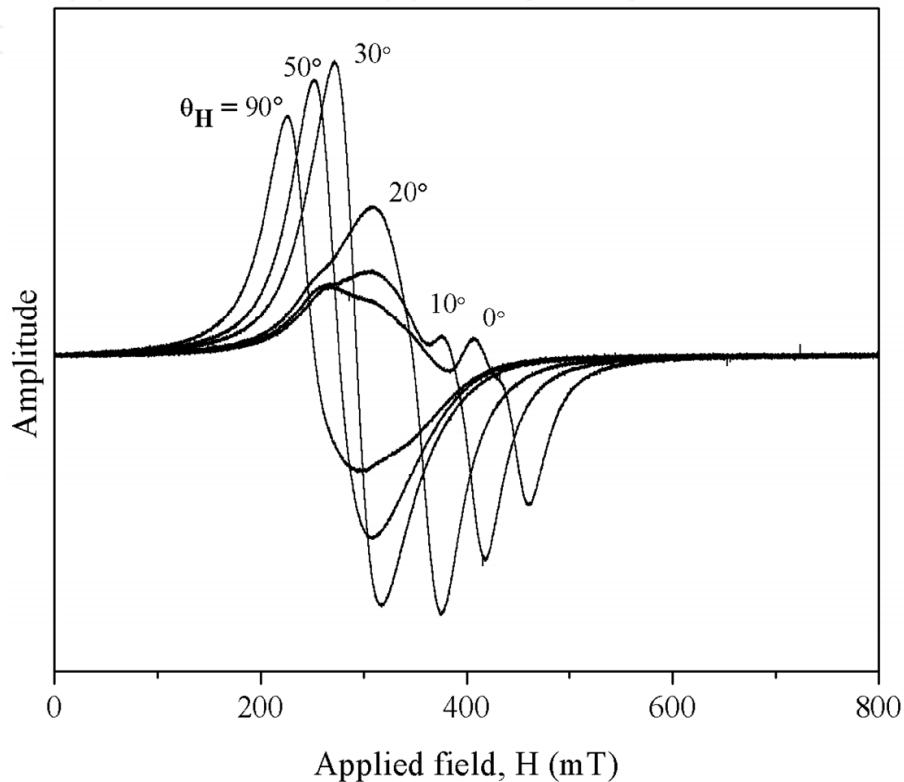

Figure 4. Room temperature FMR spectra of [SnO$_2$(46 nm)CFZ(249 nm)]$_5$ at different orientations.

The FMR spectra of [SnO$_2$(46 nm)/CZF(249 nm)]$_5$ recorded at different orientations is shown in figure 4. For $\theta_H > 20°$ there is only single resonance in the FMR spectra. Small shoulder appears at $\theta_H = 20°$. The multiple resonances appear at $\theta_H < 20°$. The relative intensity of the FMR signals is also angle dependent. As θ_H approaches 0°, the amplitude of the shoulder peaks increases at the cost of that of the main peak. The separation between the resonances also increases and the intensity of the FMR signal decreases as θ_H approaches 0°. This may be due to the prominent demagnetization effects in the perpendicular configuration. A similar behavior is exhibited by the ML with x = 86 nm. There are no multiple resonances for the ML with x = 42 nm.

Figure 5 is a representative plot of the angular dependence of A/B ratio. A/B is close to 2.1 for the perpendicular configuration and decreases as the ML approaches parallel configuration. A/B = 1 for $\theta_H \sim 30°$ showing that the spectra is symmetric at an orientation of 30° of the sample normal with the applied field. Below 30° A/B is < 1 and above 30° A/B is > 1 evidencing the variation in the intensity of the lower and upper part of the FMR spectra with θ_H.
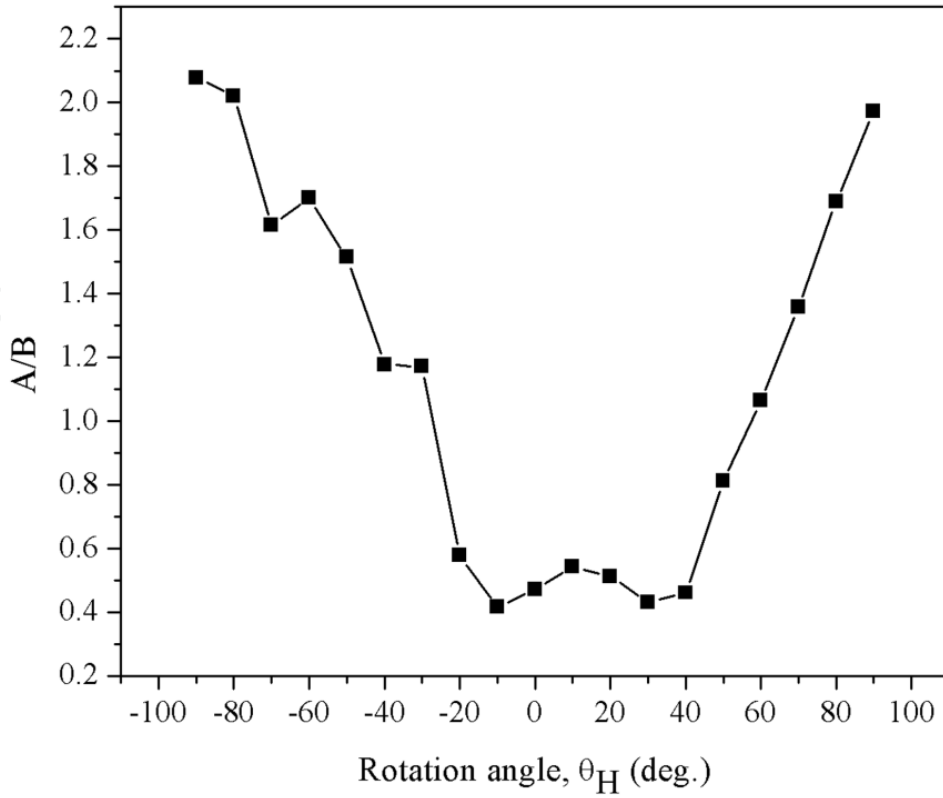
Figure 5. A representative plot of angular dependence of A/B ratio of [SnO₂(46 nm)CFZ(249 nm)]₅ ML.

Figure 6 depicts the angular variation of H_{res}, ΔH and I_{pp}. For all the ML there is no significant change in H_{res} and ΔH the FMR spectra for $\theta_H \geq 60°$. Below 60°, H_{res} and ΔH increase continuously. This shows that the ML is anisotropic in nature. The I_{pp} value initially increases from 0° till 40° followed by a decrease with further increase in θ_H. Thus the ML is homogeneous when placed at an orientation of 40°.

When an applied field is oriented along the film plane, H_{res} increases with decreasing thickness of the CZF layers. But H_{res} decreases with decreasing thickness of the CZF layers when the external magnetic field is oriented perpendicular to the film plane. This behavior is attributed to the decrease of the perpendicular anisotropy energy with decreasing CZF thickness [22]. The difference between the resonance fields in the parallel and perpendicular configuration decreases with decreasing CZF thickness evidencing the fact that the ML with x = 42 nm is relatively less anisotropic compared to the ML with x = 249 and 83 nm.

In the perpendicular configuration, the ML with x = 249 nm exhibits multiple resonances presumably due to the presence of spin waves. The spin wave resonance spectrum at RT and HT for ML with x = 249 nm were initially analyzed using the dispersion relation developed by Kittel as follows [23]

$$H_n = H_0 - \Lambda M_0 \left(\frac{\pi}{L}\right)^2 n^2 \tag{1}$$
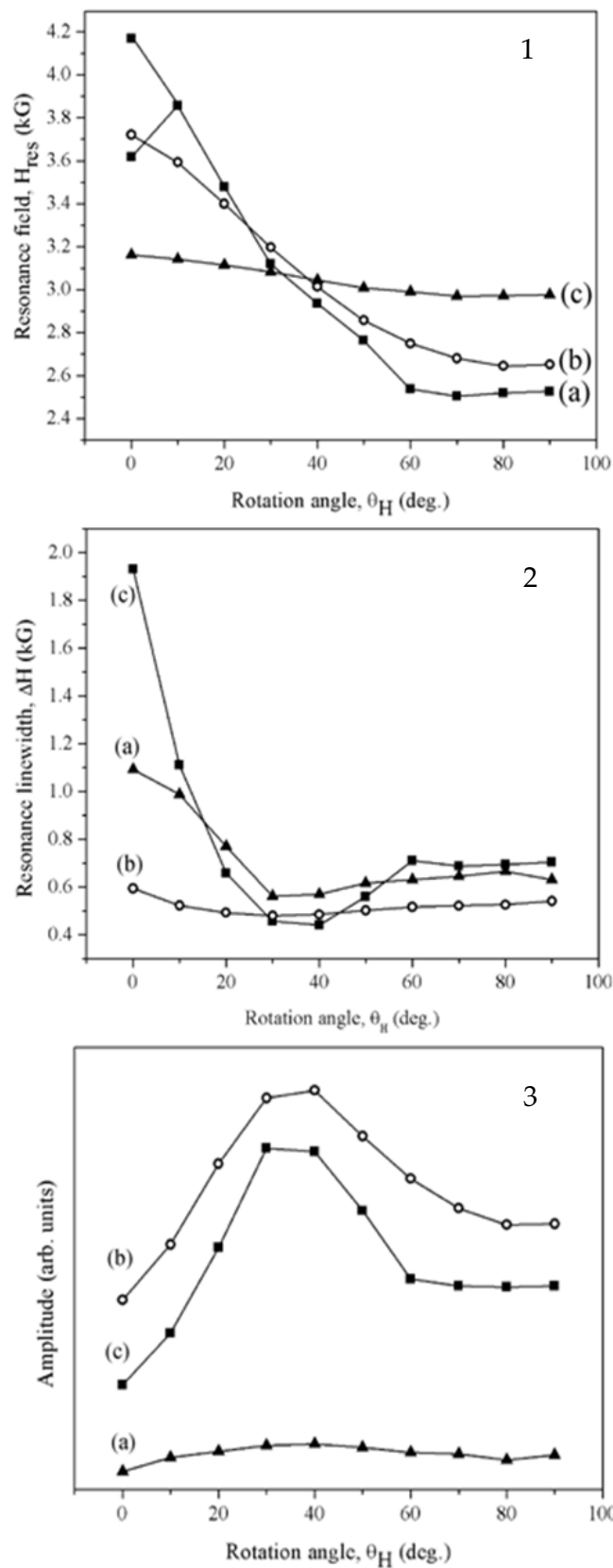
where $\Lambda = \frac{2A}{M_0^2}$

Figure 6. Angle dependence of resonance field (1), resonance linewidth (2) and amplitude (3) of [SnO$_2$(46 nm)CFZ(x nm)]$_5$ for x = 249 (a), 83(b) and 42 nm (c).

Here H$_n$ is the position of the nth mode of the spin wave resonance, H$_0$ is the position of the FMR resonance, L is the thickness of the sample, M$_0$ is the magnetization of the film, n is an odd integer and A is the exchange constant. This relation is valid for uniformly magnetized film. The results obtained do not fit well into the Kittel model where H$_n$ is plotted against n^2. They rather exhibit a linear behavior with n.

According to Portis model [24] for films with non uniform magnetic profile, the magnetization shows a parabolic drop away from the center of the film. The spin wave modes are given by the following relation

$$H_n = H_0 - \frac{4M_0}{L}(4\pi\epsilon)^{1/2}\left(n + \frac{1}{2}\right)$$

(2)

Here ϵ is the distortion parameter in the film.
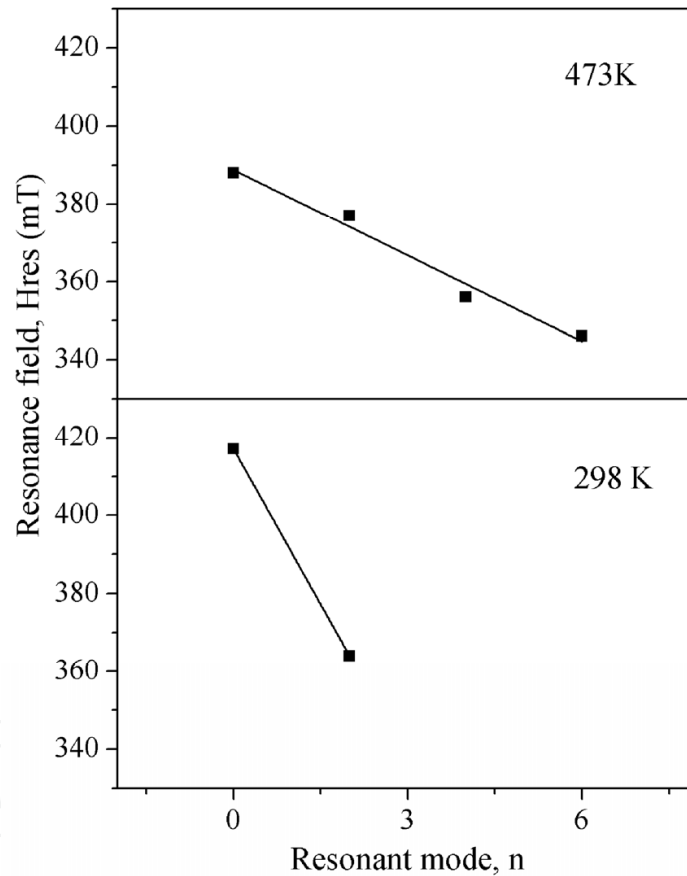

Figure 7. Variation of resonance field with the mode number according to Portis model.

Portis considered that the pinning in the film arises due to non uniform magnetization in the film. This model proposes a linear relation between H$_n$ and n. Also from the above equation, the difference between the resonance modes decreases with decrease in magnetization.

Figure 7 shows the linear fits corresponding to Portis model. The exchange constant is proportional to the slope of the line. The slope of the line decreases with increasing temperature. Hence the exchange constant decreases with increasing temperature leading to

weak coupling and hence lower magnetization. Also, the separation between the resonance modes decreases at higher temperatures, indicating a decreasing magnetization.

The effective magnetization ($4\pi M_{eff}$) and effective g value (g_{eff}) calculated using the Kittel's relations are listed in table1. At room temperature $4\pi M_{eff}$ increases and g_{eff} decreases with increasing CZF thickness. This may be due to increasing FM layer thickness [25]. The various factors which can account for deviation of g_{eff} from that of the free electron are spin orbit coupling, coupling at the interfaces etc [26].

x (nm)	H_{res} (kG)		ΔH_{res} (kG)	g ($\pm$ 0.01)		$4\pi M_{eff}$ (Oe)	g_{eff}	ΔH (G)	
	$\theta_H = 90°$	$\theta_H = 0°$		$\theta_H = 90°$	$\theta_H = 0°$			$\theta_H = 90°$	$\theta_H = 0°$
42	2.977	3.165	0.188	2.21	2.08	125.76	2.16	631	750
86	2.649	3.720	1.071	2.48	1.77	728.39	2.19	541	590
249	2.526	3.633, 4.173	1.107, 1.647	2.60	1.81, 1.58	754.41, 1132.88	2.28, 2.14	703	1930

Table 1. FMR parameters for [SnO$_2$(46 nm)/ CZF (x)]$_5$ ML for various values of x.

The perpendicular anisotropy field H$_K$ is obtained from the following equation [27]

$$H_K = 4\pi M_S - 4\pi M_{eff} \tag{3}$$

The values of K are listed in table 2. In multilayers, there are two factors which contribute to the effective anisotropy – anisotropy due to the interfacial region (K$_S$) and anisotropy due to the bulk volume of the magnetic layer (K$_V$). The relation is given as follows [28]

$$K = K_V + 2\frac{K_S}{x} \tag{4}$$

Where x is the thickness of the magnetic layer. The factor of 2 in the second term on the (r. h.s) of the equation is due to an assumption that the magnetic layer is bound by identical interfaces on either side. When (K.x) is plotted against t (figure 8), the slope gives the value of K$_V$ and the intercept gives the value of K$_S$. The negative slope indicates a negative volume anisotropy which tends to confine the magnetic moment in the plane of the film [29]. The intercept at x = 0 gives positive value of K$_S$ which tends to align the magnetic moment perpendicular to the surface of the film. The intercept on the x axis gives the thickness at which the contribution from K$_V$ outweighs that from K$_S$. From the figure, the intercept on x axis is found to be 56 nm. Thus below 56nm, major contribution comes from interfaces. The K$_S$ and K$_V$ values obtained from the plot are 194980 and -3671 erg/cm^3

The value of K changes from positive to negative as the thickness of CZF increases (figure 8). Negative values of K indicates in-plane anisotropy [30]. Thus with increasing CZF thickness, the direction of magnetization is confined to the plane of the sample surface. The thickness value at which the anisotropy changes sign is 56 nm. The perpendicular anisotropy for small values of x may be due to the lattice mismatch at the interfaces [31].
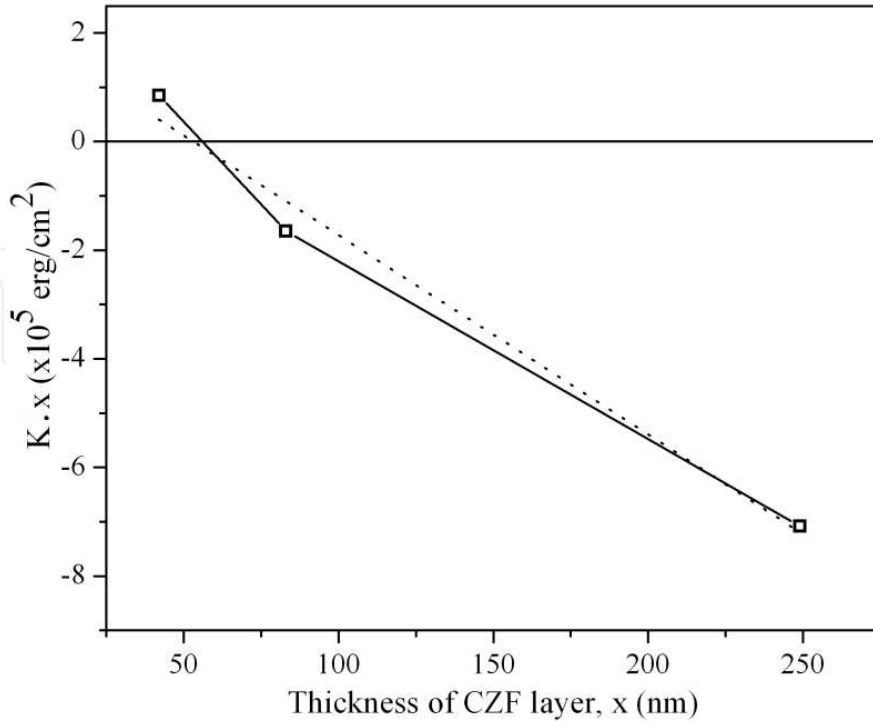
Figure 8. (K.x) vs x plots for [SnO₂(46 nm)CFZ(x nm)]₅ ML for x = 43, 83 and 249 nm.

Gilbert damping is a spin relaxation phenomenon in magnetic systems which controls the rate at which the spins reach equilibrium. Spin-orbit coupling [32], non-local spin relaxations like spin wave dissipation [33,34] and disorder present in the materials are the major factors causing Gilbert damping. The damping parameter α values are 0.0096, 0.0083 and 0.0108 for x = 42, 83 and 249 nm respectively. The increase in α value with CZF thickness indicates the increase in the damping of spins with increasing thickness.

x	α		K_1
(nm)	$\theta_H = 90°$	$\theta_H = 0°$	$(10^3 \, erg/cm^3)$
42	0.049	0.057	2.027
86	0.041	0.045	-1.989
249	0.053	0.146	-2.845, -1.254

Table 2. Damping and anisotropy parameters for or [SnO₂(46 nm)/ CZF (x)]₅ ML for various values of x.

The temperature dependent FMR studies in the temperature range 133- 473K were carried out on the ML. Figure 9 shows the FMR spectra of the ML at various temperatures. The change in line shape indicates change in the magnetic interaction with increasing temperature.

Figure 10 shows the variation of I_{PP} with temperature in the parallel configuration. I_{PP} increases with increasing temperature for all the ML. I_{PP} of the ML with x= 42 nm exhibits a linear trend. Whereas for ML with x=83 and 249 nm, the increase is not linear. It increases slowly from 133K to 298K (RT), followed by a rapid increase with temperature in the

temperature range RT- 473K. From 133K to 250K there is no significant difference in amplitude for ML with x= 83 and 249 nm. At temperatures above RT the amplitude of ML with x= 83 nm is higher than that of ML with x = 249 nm.
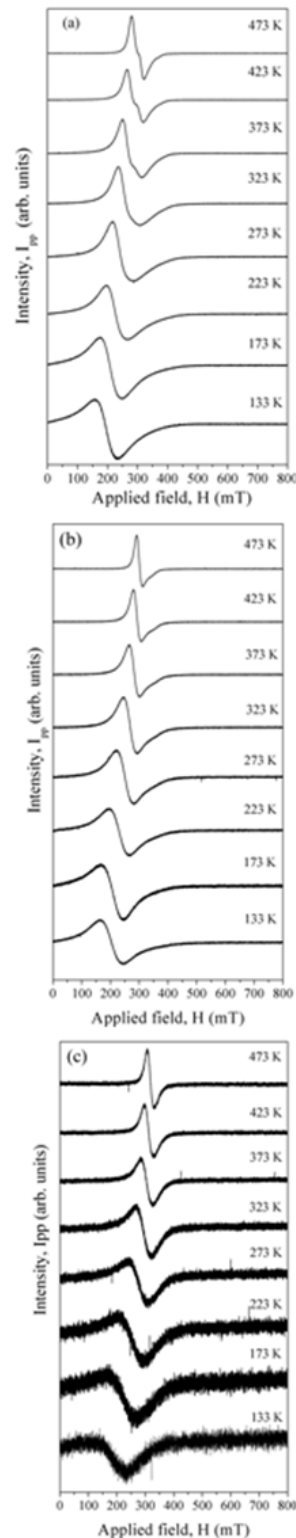

Figure 9. FMR spectra of [SnO$_2$(46 nm)CFZ(x nm)]$_5$ ML at various temperatures for x = 249 (a), 83 (b) and 42 nm (c)in the parallel configuration.
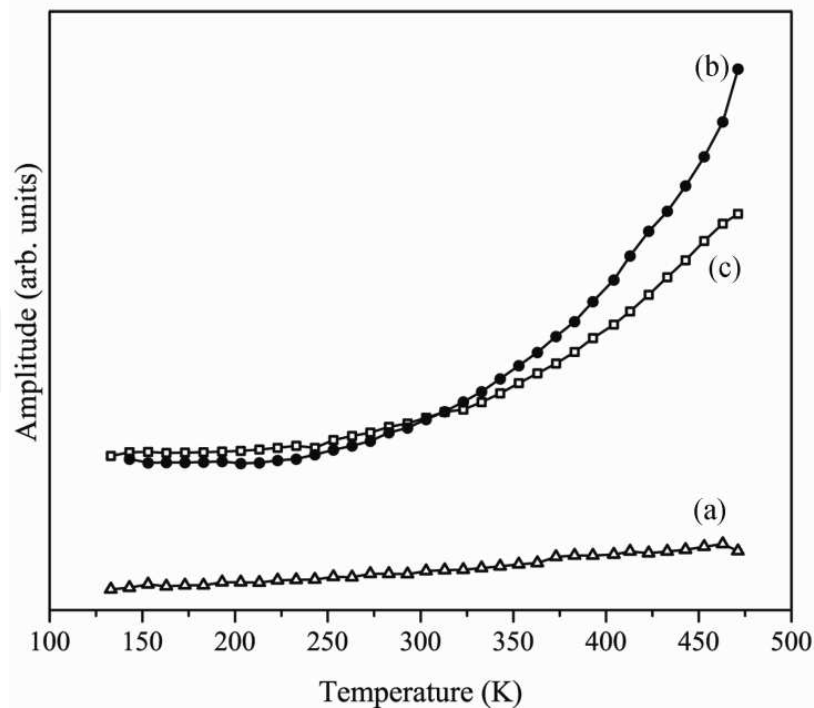
Figure 10. Temperature dependent amplitude of [SnO$_2$(46 nm)CFZ(x nm)]$_5$ for x = 249(a), 83(b) and 42 nm (c).

Variation of ΔH with temperature in the parallel configuration is displayed in figure 11. The width of the FMR spectra increases continuously with decreasing temperature for x= 42 nm. For x = 83 nm it decreases with temperature and saturates at ~ 215 K . Whereas for x = 249 nm it begins saturating at ~ RT presumably due to freezing of spins. The H$_{res}$ increases with increasing temperature (figure 12) in all the ML presumably due to increasing internal field at low temperatures. The ML with x = 249 nm exhibits a linear dependence in the entire temperature range whereas the ML with x = 83 and 42 nm exhibit saturating tendency at higher temperatures in the parallel configuration. This may be an interfacial effect. For x = 42 nm the ratio of spins at the interfaces to the spins in the bulk is high. Whereas for x = 83 and 249 nm the ratio is lower. Hence the contribution from the bulk of the film becomes significant than that from the interfaces. The saturating tendency at high temperatures for the ML with x = 83 and 42 nm shows that even at higher temperatures, the thermal energy is not sufficient to unlock the spins at the interfaces.

Similar behavior is observed for CZF thin films [12]. The increase in saturation temperature with increase in CZF thickness could be due to the interlayer coupling.

The change of slope of ΔH indicates a change in the kind of magnetic interactions in the ML. The line shape of the FMR spectra also changes around the same temperature. The curvature of the temperature dependent of ΔH plot changes as x increases from 42 to 249 presumably due to increase in active to dead layer ratio. Decreasing trend in I$_{pp}$ and H$_{res}$ and increasing trend in ΔH with decreasing temperature is a signature of superparamagnetism [35]. The resonance field of a given particle includes contribution from magneto crystalline anisotropy field and demagnetizing field.
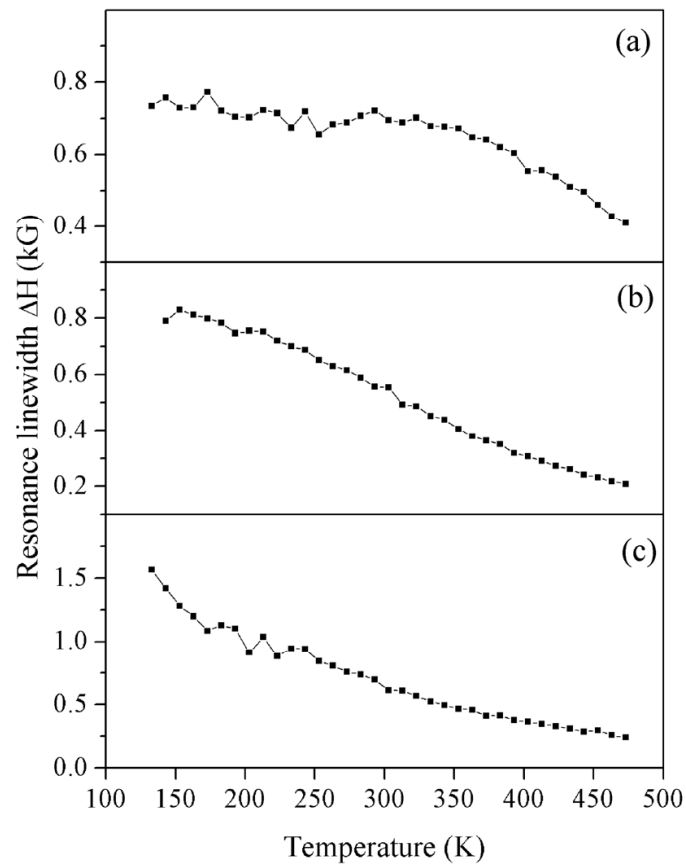
Figure 11. Temperature dependent resonance linewidth of [SnO₂(46 nm)CFZ(x nm)]₅ for x = 249(a), 83(b) and 42 nm (c).

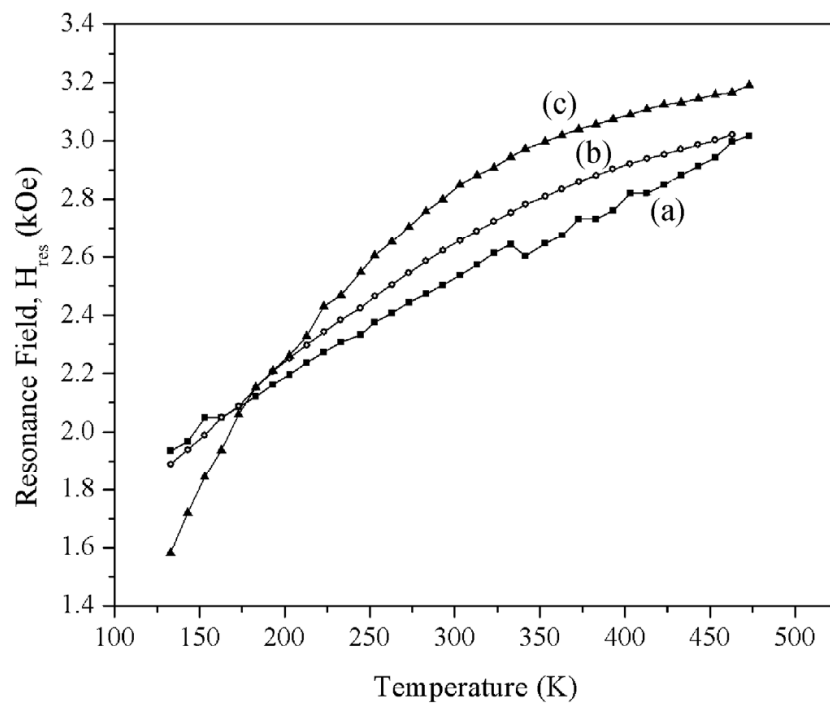**Figure 12.** Temperature dependent resonance field, H$_{res}$, in the parallel and perpendicular configuration of [SnO₂(46 nm)CFZ(x nm)]₅ for x = 249(a), 83(b) and 42 nm (c).

For a system containing randomly oriented particles, the magnetic resonance signal is broad. At high temperatures where k_bT is much greater than the anisotropy barriers the thermal fluctuations of the magnetic moments reduces the angular anisotropy of the resonance fields and the linewidth of individual nanoparticle [36] resulting in a superparamagnetic resonance (SPR) spectra in the case of nanoparticles. At low temperatures the particle moments are unable to overcome the local anisotropy barriers and, thus, become trapped in metastable states (blocking phenomenon). This results in broad resonance spectra with linewidth comparable to that of the resonance field.

A characteristic feature of SPR is that at low temperatures, ΔH is almost equal to the value of H_{res}. For the ML with x = 42 nm around 40% of CZF layer is dead. The diffused region consists of fine particles of CZF dispersed in SnO₂ matrix. Hence the SPR phenomenon is pronounced for this ML. Whereas for ML with x = 83 and 249 nm, the thickness of the diffused region is small compared to that of the bulk CZF layer. Hence the value of ΔH at low temperatures is not same as that of H_{res}.

FMR susceptibility is estimated by calculating the double integrated intensity i.e. area under the absorption curve in FMR is proportional to the concentration of spins. Figure 13 shows temperature dependence of ESR susceptibility in the parallel configuration for *[SnO₂(46 nm)CFZ(x nm)]₅* ML. It initially increases with decreasing temperature, reaches a maximum and then decreases with further decrease in temperature evidencing the superparamagnetic behavior. The width of the transition is large due to the wide spread of blocking temperatures.
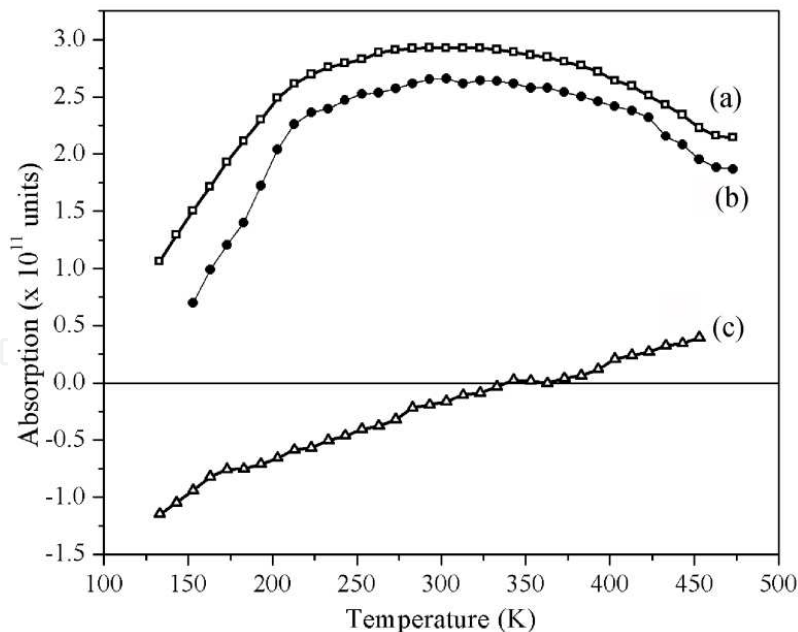

Figure 13. Variation of FMR susceptibility, χ_{FMR} with temperature of [SnO₂(46 nm)CFZ(x nm)]₅ ML for x = 249 (a), 83 (b) and 42 nm (c).

For ML with x = 42 nm, χ_{FMR} decreases continuously with decrease in temperature down till 183 K. The negative absorption is due to the fact that the area under the lower part of the

FMR curve is greater than that of the upper part. The Curie- Weiss law does not fit $1/\chi_{FMR}$ vs T plot due to the continuous curvature in the entire temperatures range.

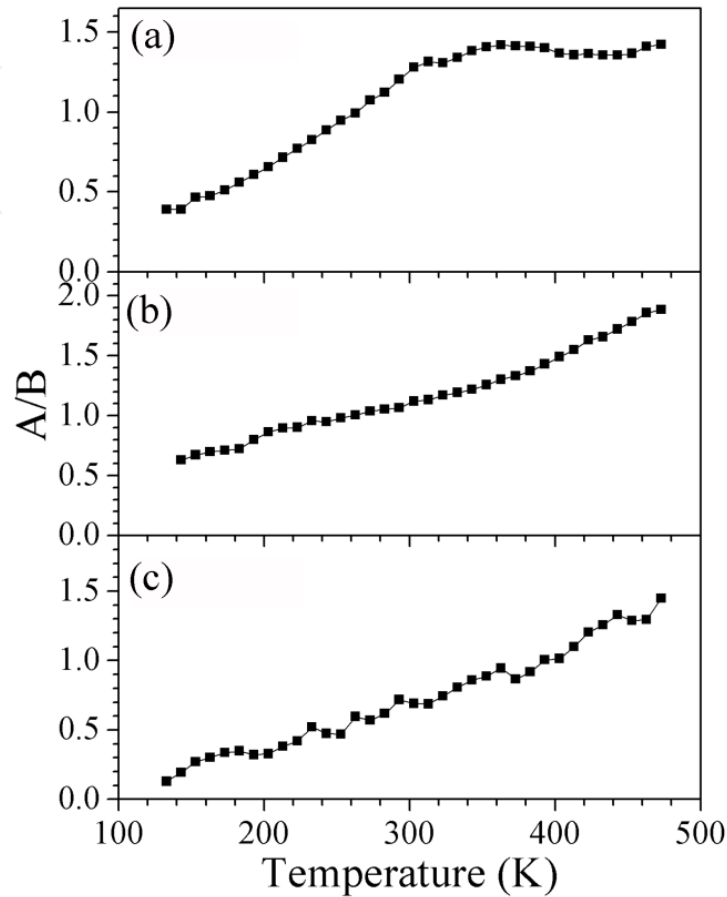**Figure 14.** Variation A/B ratio with temperature of [SnO$_2$(46 nm)CFZ(x nm)]$_5$ ML for x = 249(a), 83(b) and 42 nm (c).

Figure 14 shows the A/B ratio with temperature for these ML. It decreases almost linearly with decreasing temperature from 400 to 200 K for the ML with x = 42 nm. Below 200 K there is a change in slope. The temperature dependence of A/B ratio exhibits different slopes in different temperature region for the ML with x = 83 nm. Whereas for the ML with x = 249 nm, there is no significant change in the A/B ratio in the temperature range between 500 and 350 K. Below 350 K the ratio decreases continuously. The temperature at which the slope for A/B ratio changes matches with that of temperature dependence of linewidth.

Temperature dependence of FMR spectra of these ML in the perpendicular configurations is displayed in figure 15. The resonance field shifts towards higher values with decreasing temperature. This is accompanied with decrease in intensity and increase in line width. This indicates that AFM interactions dominate as temperature decreases in the perpendicular configuration.
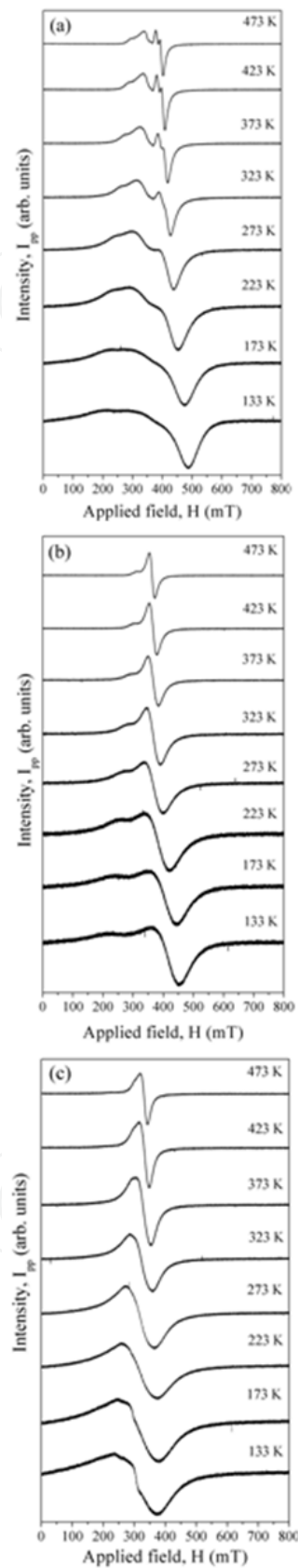
Figure 15. FMR spectra of [SnO$_2$(46 nm)CFZ(x nm)]$_5$ at various temperatures in the perpendicular configuration for x = 249 (a), 83 (b) and 42 nm (c).

Figure 15(a) also shows the variation in the positions of the multiple resonances for x = 249. They are narrow and closely spaced at 473 K. As temperature decreases, the FMR peaks broaden and move away from each other with decreasing temperature. The peak at the lower field moves further towards lower field and the one at the higher field moves further towards higher field. This is a clear indication of existence of both FM and AFM phase. The relative intensity of the peak at higher field decreases and that of the one at lower field increases with decreasing temperature. The distance between the peaks increases with decreasing temperature. This indicates increase in phase separation with decrease in temperature.

I_{pp} value in the perpendicular configuration is lower than that in the parallel configuration at all temperatures. However, the trend remains the same in both parallel and perpendicular configurations. The ΔH value in the perpendicular configuration is not very much different from that in the parallel configuration for the ML with x = 42 and 83 nm (figure 16). On the other hand, ΔH for x = 249 ML is much higher in the perpendicular configuration.
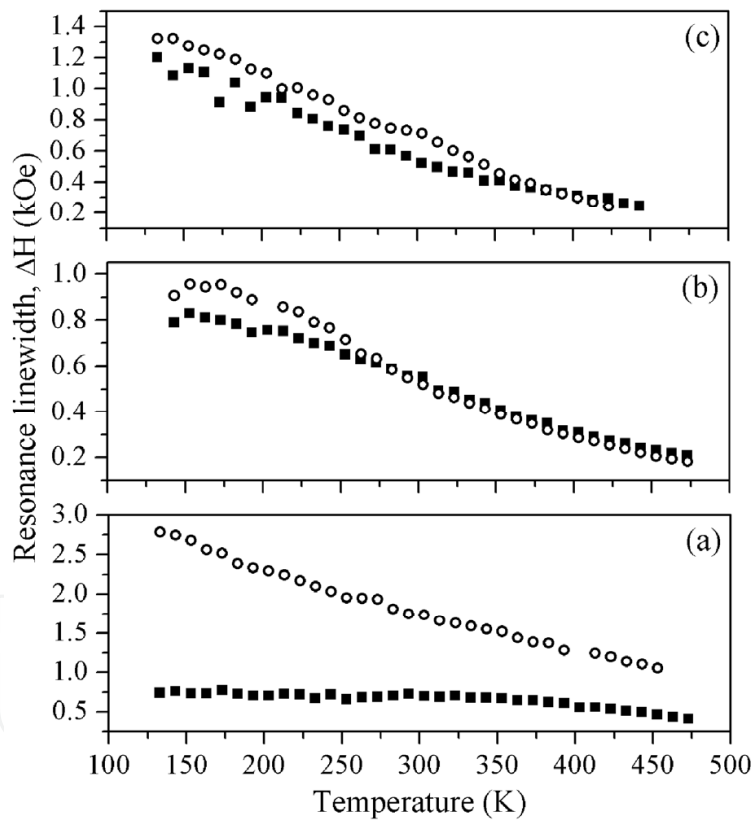

Figure 16. Temperature dependent resonance linewidth in the parallel (full circle) and perpendicular (open circle) configuration of [SnO₂ (46 nm)CFZ(x nm)]₅ for x = 249(a), 83(b) and 42 nm (c).

Figure 17 shows the variation of H_{res} in the parallel and perpendicular configuration. Unlike the parallel configuration, the resonance field increases with decreasing temperature in the perpendicular configuration for ML with x = 249 and 83 nm. H_{res} remains insensitive to temperature in the range 300- 473K. Below 300 K it increases with further decrease in temperature.
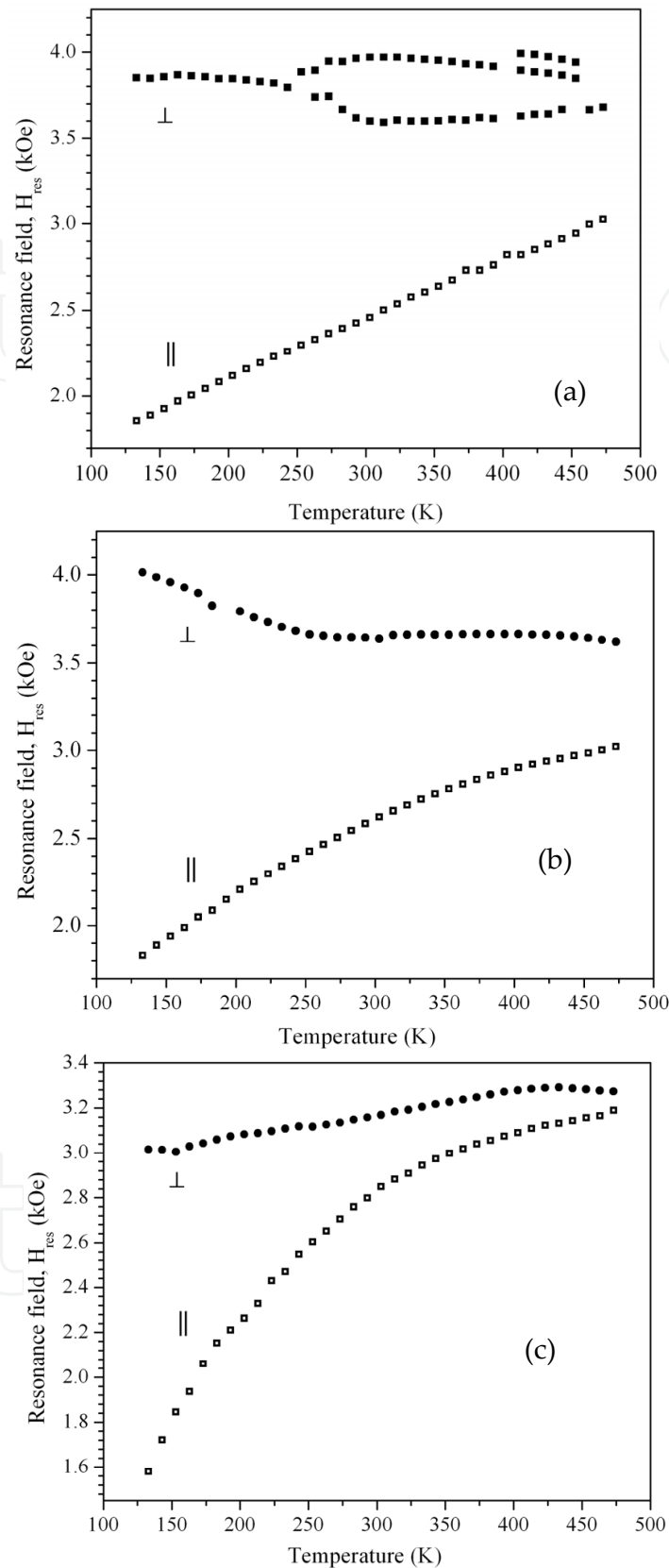
Figure 17. Temperature dependent resonance field, H_{res}, in the parallel and perpendicular configuration of [SnO$_2$(46 nm)CFZ(x nm)]$_5$ for x = 249 (a), 83 (b) and 42 nm (c).

Whereas for the ML with x = 42 nm, initially there is a small increase in H_{res} as temperature decreases from 473 to 433 K. Below 433 K it decreases continuously. At all temperatures, H_{res} is less sensitive to temperature in the perpendicular configuration than in the parallel configuration.

For all the ML, the FMR susceptibility increases with decreasing temperature in the perpendicular configuration. The effective magnetization is a measure of net magnetization within the ML. Figure 18 shows the variation of effective magnetization with temperature. It increases with decreasing temperature for all ML.
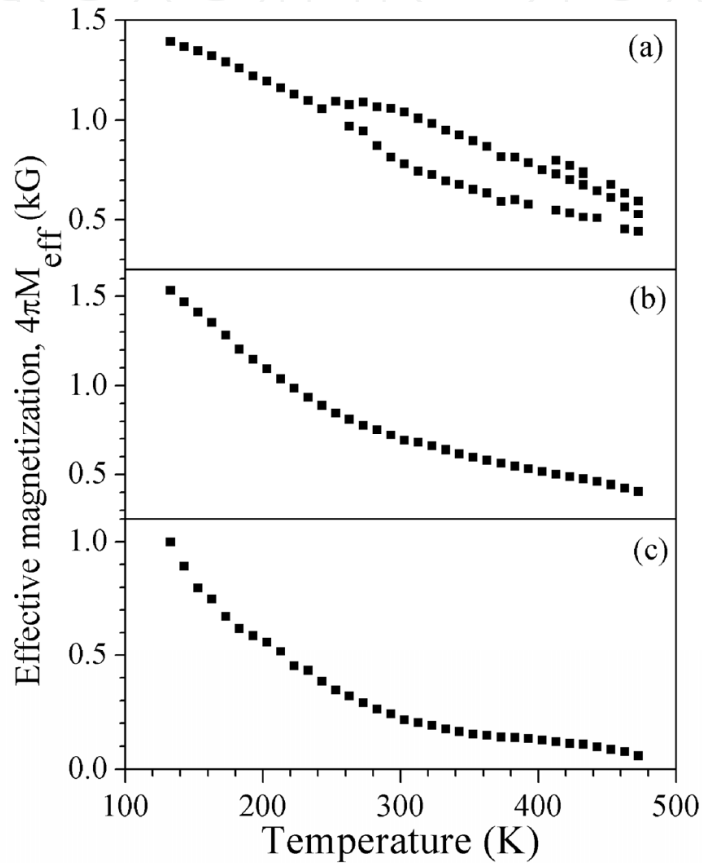

Figure 18. Variation of effective magnetization with temperature for [SnO₂ (46 nm)CFZ(x nm)]₅ ML for x = 249(a), 83(b) and 42 nm (c).

Figure 19 is a representative graph of [SnO₂ (46 nm)/ CZF(249 nm)]₅ ML showing the variation of FMR susceptibility with temperature in both parallel and perpendicular configurations. Unlike the parallel configuration, χ_{FMR} in the perpendicular configuration increases continuously with decreasing temperature.

The FMR spectra were recorded at different orientations of the normal to the sample with the applied field (θ_H). The rotational dependence of FMR spectra was measured at 133, 298 (room temperature) and 473 K. At all temperatures the resonance field increases continuously as θ_H decreases exhibiting uniaxial anisotropy. For the ML, the difference between ΔH values in the parallel and perpendicular configuration increases with

decreasing temperature. This shows increasing anisotropy with decreasing temperature. The multiple resonance for the ML with x = 249 is prominent at 298 and 473 K (figure 20(a)). For ML with x < 249 nm, the absence of multiple resonances even at high temperatures indicates absence of interlayer coupling. At all temperatures the ΔH_{res} is highest for the ML with x = 249 nm. These multiple resonances disappear with decreasing temperature.
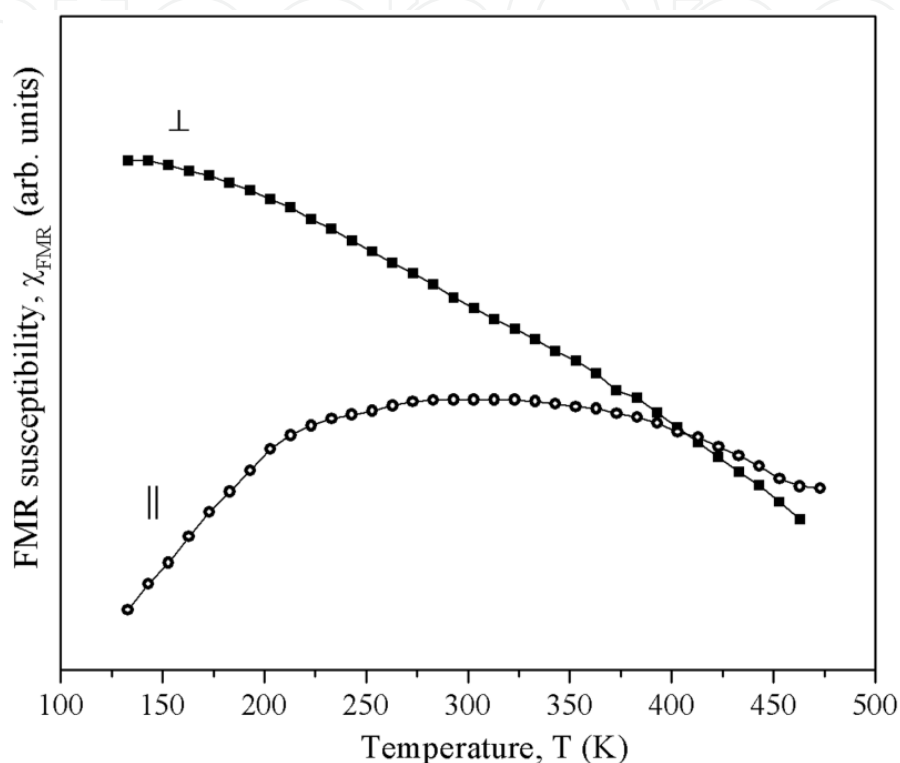

Figure 19. Representative plot of the FMR susceptibility, FMR of [SnO₂ (46 nm)CFZ(249 nm)]₅ ML in parallel and perpendicular configuration.

At room temperature, ΔH shows a minimum ~ 30-40° (figure 21). I_{pp} shows maximum around the same value. Hence the sample has an easy axis of magnetization at that inclination. At 473 and 298 K its intensity initially increases, reaches a maximum and then decreases with decreasing θ_H. Whereas at 133 K, I_{pp} values remains constant initially then decreases continuously with decreasing value of θ_H.

Another evidence for decreasing anisotropy with decreasing x is shown in figure 21. At 473 K, ΔH for the ML with x = 249 nm initially increases, exhibits a minimum ~ 40° and then increases continuously with further increase in θ_H . Whereas for the ML with x = 83 nm, with increasing θ_H, ΔH value remains constant till certain angle then decreases continuously. On the other hand the ΔH value for the ML with x = 42 nm, the ΔH value continuously decrease reaches a minimum and then increases with increasing θ_H. The occurrence of minimum in ΔH may be due to existence of regions with different effective magnetization values due to inhomogeneous nature of the sample [37]. The minimum in ΔH shifts towards higher angle with decreasing x. Similar behavior is observed at 298 K for all the ML. With decreasing
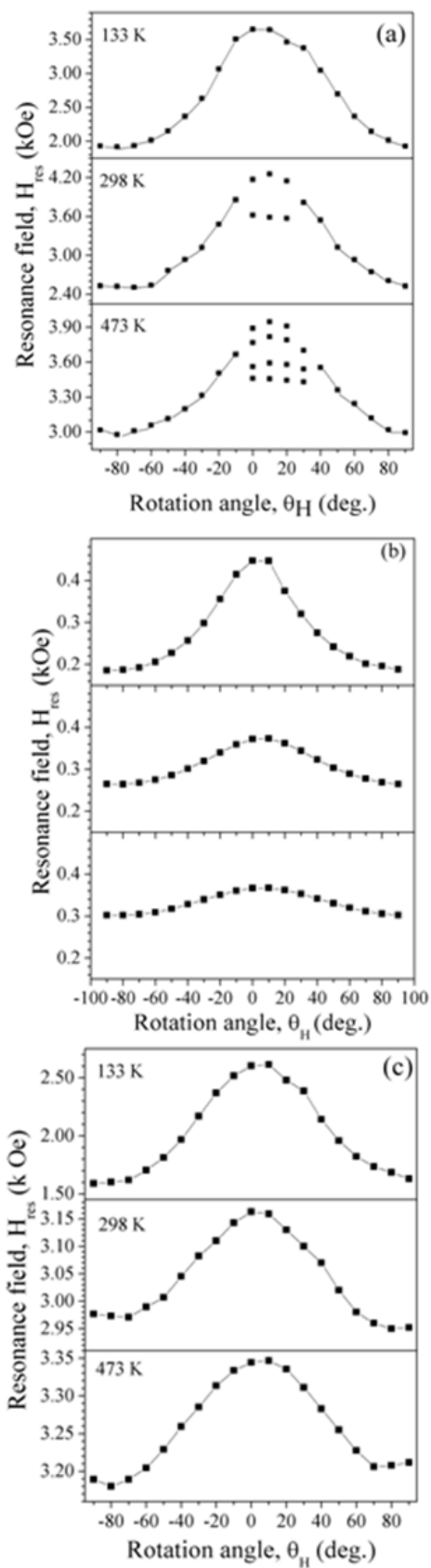
Figure 20. Rotational dependence of resonance field, H_{res}, at various temperatures for $[SnO_2$ (46 nm)CFZ(x nm)]$_5$ ML where x = 249(a), 83(b) and 42 nm (c).
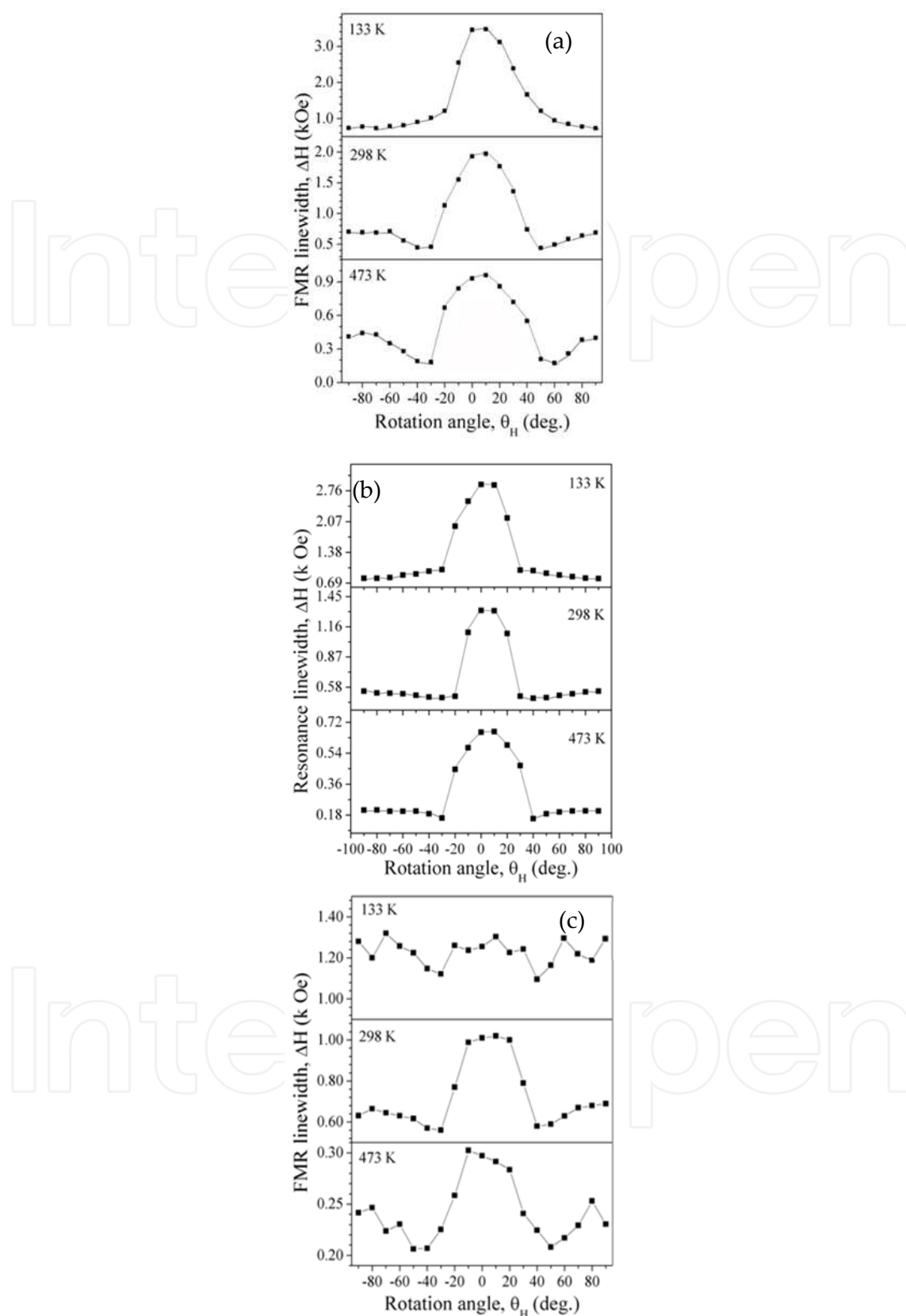
Figure 21. Rotational dependence of resonance linewidth, ΔH, at various temperatures for [SnO₂ (46 nm)CFZ(x nm)]₅ ML for x = 42(a), 83(b) and 249 nm (c).

temperature, the curvature of the angle dependent linewidth changes. At 133 K, for x = 249 nm, the minima vanishes and ΔH increases continuously with increasing θ_H. For the ML with x = 83 nm, the curvature is reversed at 133 K. It increases with increasing θ_H, attains a maximum value at ~ 40° and then decreases. On the contrary there is no significant change in ΔH for the ML with x = 42 nm. Thus at 133 K, x = 249 nm ML is more anisotropic than the ML with x = 42 and 83 nm.

3.2. Effect of spacer layer thickness

The effect of thickness of spacer (SnO_2) layer was studied on 3 sets of samples with varying thickness of the SnO_2 layer. The total number of bilayers is 5 and individual CZF layer thickness is 83 nm for all the samples. The ML samples were $[SnO_2(x\ nm)\ CZF(83\ nm)]_5$ ML for x = 46 , 115 and 184 nm .

Stack of alternate dark and light layers are evident from the FESEM images (figure 22). The dark columnar layers correspond to CZF and the light layers correspond to SnO_2. The variation in the thickness ratio between SnO_2 and CZF is also clearly visible from these images. The absence of fringes in XRR spectra may be due to large thickness of the ML stack.
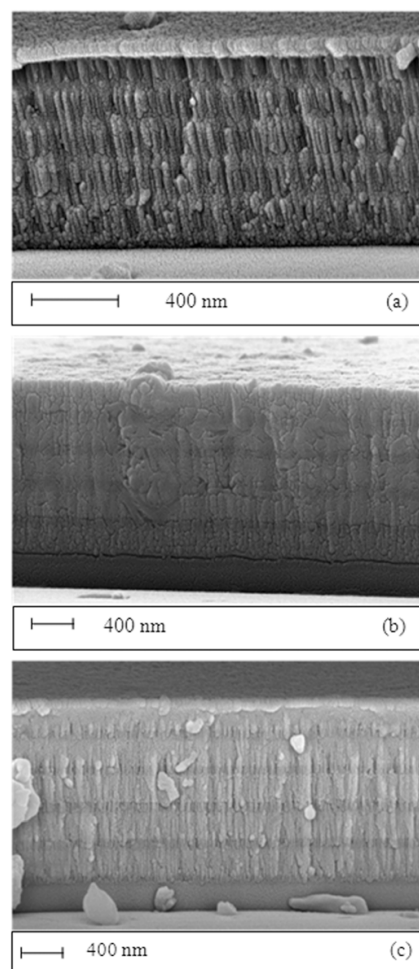

Figure 22. FESEM images of $[SnO_2(x\ nm)\ CZF(83\ nm)]_5$ ML for x = 46 (a), 115 (b) and 184 nm (c).

FMR studies were carried out at different temperatures and by varying the angle θ_H between the film normal and the direction of the applied field. Figure 23 shows the first derivative of the FMR absorption spectra of the ML at room temperature in parallel (θ_H = 90°) and perpendicular (θ_H = 0°) geometry, normalized to the volume of the CZF layers. I_{PP} increases as the spacer (SnO₂) thickness increases from x = 46 to 115 nm followed by a decrease for x = 184 nm. The peak to peak linewidth (ΔH) is sensitive to inhomogenieties, surface roughness, internal field etc. The χ_{FMR} is estimated by calculating double integrated intensity (DI). Both ΔH and DI follow a trend similar to that of I_{PP} with increase in spacer layer thickness. This behavior may be attributed to the oscillation in the exchange coupling across the NM layer due to quantum interference of the electron waves reflected from the interfaces. The A/B ratio is 0.82, 0.74 and 0.79 for x = 46, 115 and 184 nm respectively. The asymmetry ratio is not very different from each other. For the ML with x = 115 nm, the upper part of the FMR signal rises steeply whereas the rise is relatively slow for the lower part indicating a negative anisotropy.
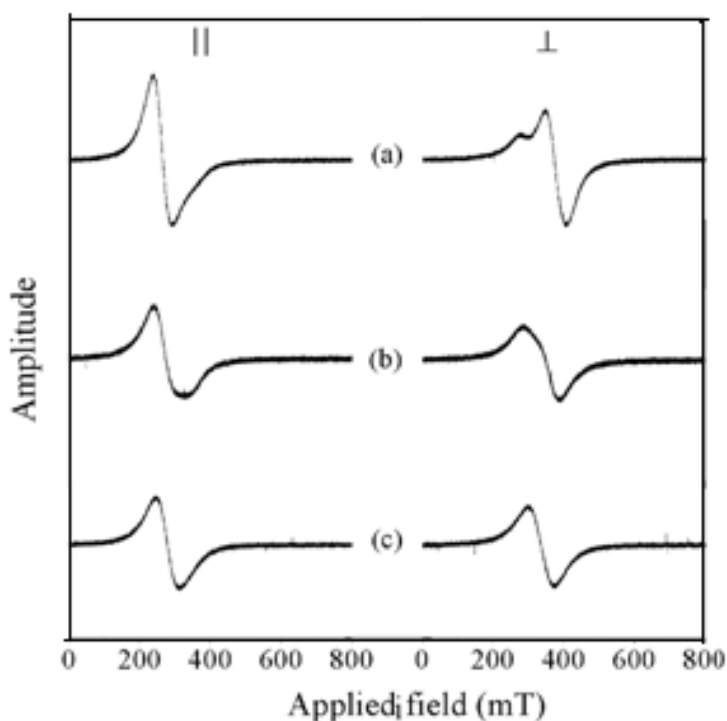

Figure 23. Room temperature FMR spectra of [SnO₂(x nm) CZF(83 nm)]₅ ML in the parallel and perpendicular configuration for x = 46 (a), 115 (b) and 184 nm (c)..

The resonance field (H_{res}) increases from 2.65 to 2.78 kG and the g value decreases from 2.47 to 2.36 with increase in SnO₂ layer thickness in parallel geometry. The shift in H_{res} to higher values might be due to the decrease in interlayer coupling strength. The H_{res} decreases and g values increases from 1.77 to 1.96 with increasing spacer layer thickness in the perpendicular geometry. This might be attributed to lower perpendicular anisotropy for well separated films [38]. The FMR parameters in the parallel and perpendicular configurations are listed in table 3. The effective magnetization decreases with increasing SnO₂ thickness.

x (nm)	H_{res} (kG)		ΔH_{res} (kG)	g (± 0.01)		$4\pi M_{eff}$ (Oe)	ΔH (G)		M_s (emu/cc CZF)
	$\theta_H = 90°$	$\theta_H = 0°$		$\theta_H = 90°$	$\theta_H = 0°$		$\theta_H = 90°$	$\theta_H = 0°$	
46	2.652	3.721	1.069	2.48	1.77	710	541	595	50
115	2.733	3.452	0.719	2.41	1.90	485	693	733	100
184	2.784	3.356	0.576	2.36	1.96	406	675	736	30

Table 3. FMR parameters of [SnO$_2$(x nm) CZF(83 nm)]$_5$ multilayers for various spacer layer thickness

The ML with x = 46 nm exhibits multiple peaks in the FMR spectrum recorded in the perpendicular configuration. This may be due to the interlayer coupling of the CZF layers mediated by the non magnetic spacer layer. When two spins are coupled across the spacer layer, they tend to precess at a frequency different from that of the rest. Hence the resonance for the coupled spins occurs at a different field. The absence of multiple splitting in the other two samples indicates lack of interlayer coupling in the magnetic layers. Apart from the multiple resonances, the asymmetry in the FMR signal in the perpendicular configuration also decreases with the increase in SnO$_2$ layer thickness. As the thickness of the spacer increases, the distance between the CZF layers increases and hence the coupling between them decreases leading to symmetrical FMR spectra. The effective magnetization value at room temperature was calculated using the Kittel's relations and are 710, 485 and 406 Oe for x = 46, 115 and 184 nm respectively.
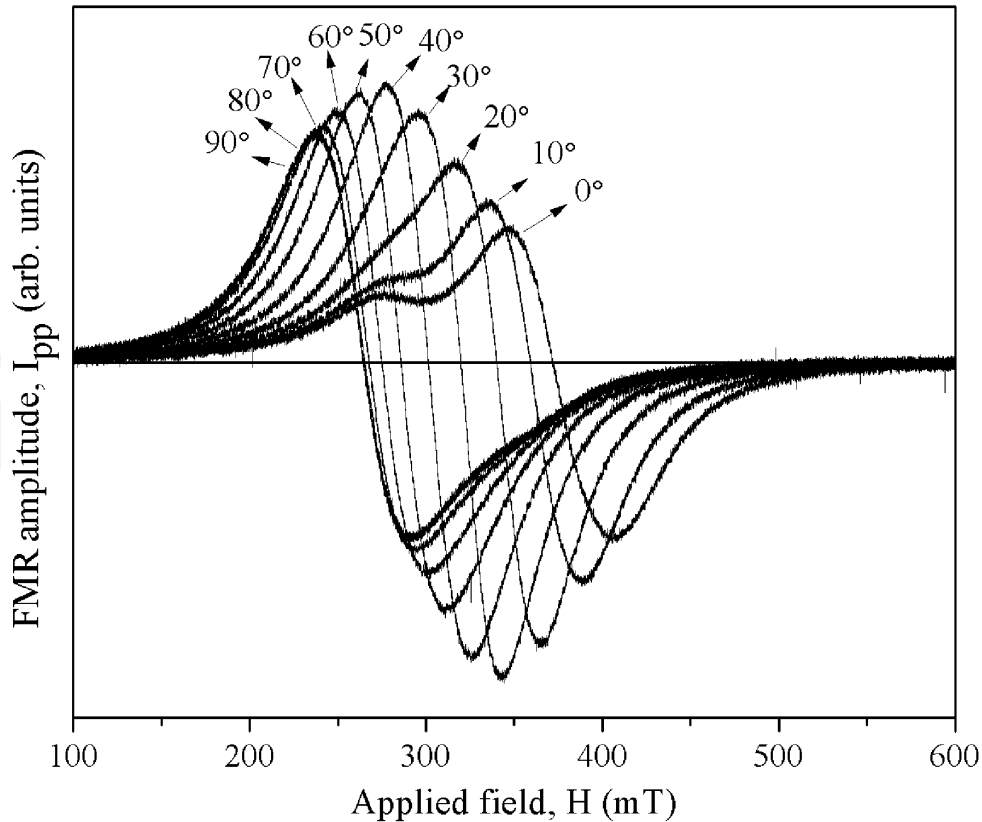

Figure 24. Room temperature FMR spectra of [SnO$_2$(46 nm)CFZ(83 nm)]$_5$ at different orientations.

The angle dependent FMR spectra are shown in figure 24. The symmetry in the FMR spectra increases as θ_H decreases from 90° to 40°. For $\theta_H > 40$° the spectra becomes asymmetric and the single FMR peak splits into two resonance peaks. With decreasing θ_H the separation of the peaks increases.

Figure 25 is a representative graph of the angular dependence of ΔH and I_{pp}. For all ML, ΔH value initially decreases till $\theta_H = 40$° and then increases till $\theta_H = 0$°. Whereas, I_{pp} increases till $\theta_H = 40$° and then decreases till $\theta_H = 0$°. This indicates that at $\theta_H = 40$°, the susceptibility of the film increases resulting in higher magnetization. This may be due to existence of regions with two different effective magnetizations. For all the samples H_{res} shifts to higher fields as the angle between the sample normal and the direction of the field (θ_H) changes from 90° to 0°. This indicates that the ML exhibits uniaxial anisotropy.
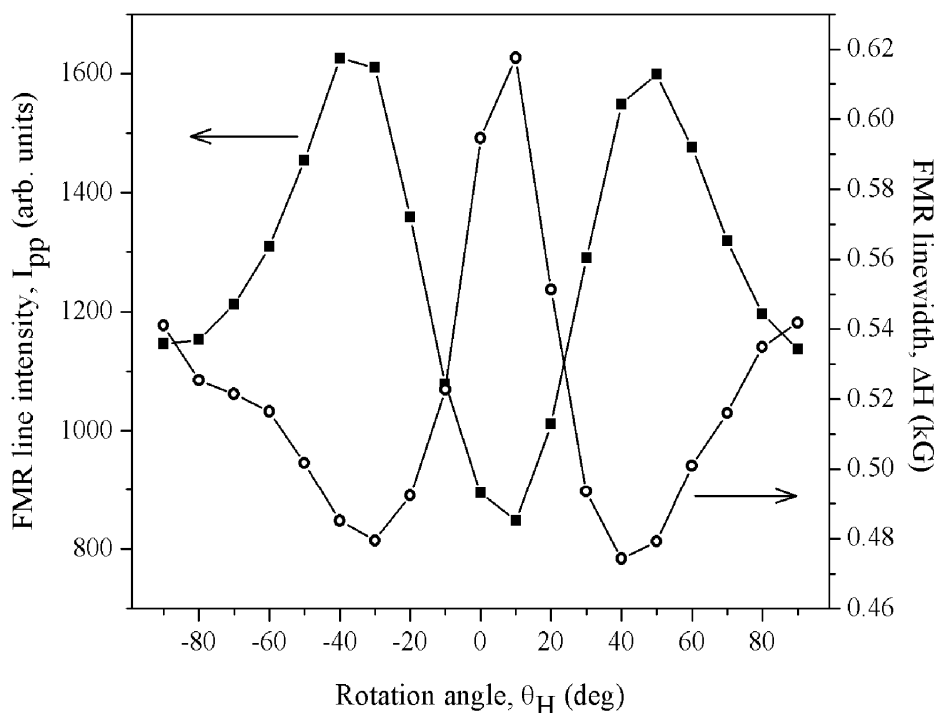

Figure 25. Variation of room temperature FMR linewidth (ΔH) and intensity (I_{pp}) of [SnO₂ (46 nm) CZF(83 nm)]₅ ML at different orientations of the film.

FMR spectra recorded at various temperatures between 133 and 473 K are shown in figure 26. The change in the lineshape with decreasing temperature evidences an evolution of a different type of magnetic interaction.

The FMR signal is asymmetric at high temperatures and the symmetry increases with decreasing temperature. In the high temperature region A/B is greater than 1 indicating that the upper part of the FMR spectrum is of higher intensity than the lower half and indicates the presence of dispersive component in the ML. Figure 27 shows the variation of A/B with temperature.
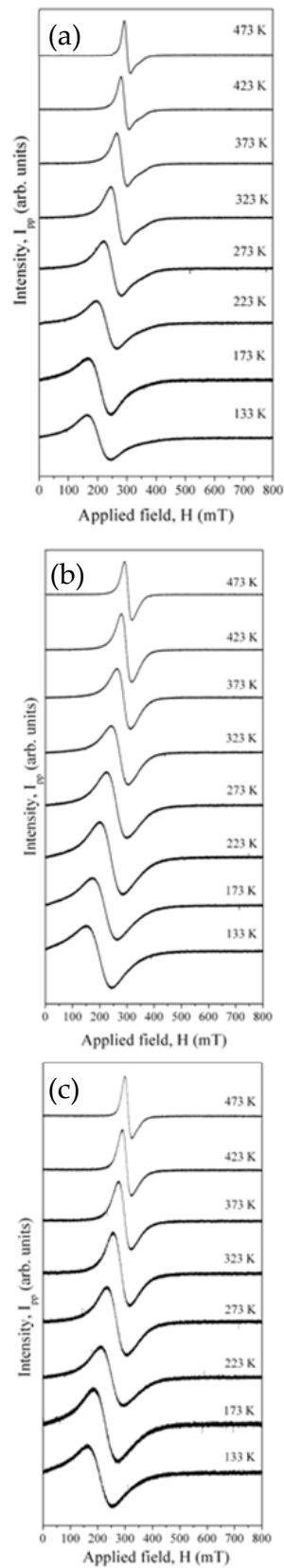
Figure 26. FMR spectra of $[SnO_2 (x\ nm)\ CZF(83\ nm)]_5$ ML recorded at various temperatures in parallel configuration for x = 46 (a), 115 (b) and 184 (c).

The I_{pp} value decreases with decreasing temperature. The increase in ΔH at lower temperatures indicates the large spin relaxation times and hence large coercivity at low temperatures (figure 28(a)).

The decreasing trend in I_{pp} and H_{res} and increasing trend in ΔH with decreasing temperature is a signature of superparamagnetism. Figure 29 shows variation of FMR susceptibility, χ_{FMR} as a function of temperature. It initially increases, reaches a maximum and then decreases with decreasing temperature confirming the superparamagnetic nature of the ML. Figure 30 shows the temperature dependent FMR spectra in the perpendicular configuration. All the ML samples exhibit multiple resonances. The resonances broaden and the separation between them increases with decreasing temperature. The intensity of the peak at lower field side increases and that at higher field side decreases with decreasing temperature.

The behavior of ΔH and I_{pp} is same as that of $\theta_H = 90°$. The difference between ΔH in both the configurations is negligible in the HT region for all the samples. The substantial difference occurs at low temperatures (figure 31(a)). This may be due to the presence of magnetic inhomogeneities in the ML [39]. In the parallel configuration H_{res} decreases with decrease in temperature indicating strengthening of FM interactions. Whereas in the perpendicular configuration it is less sensitive to temperature in the HT- RT range, then increases slowly with decrease in temperature (figure 31 (b)).
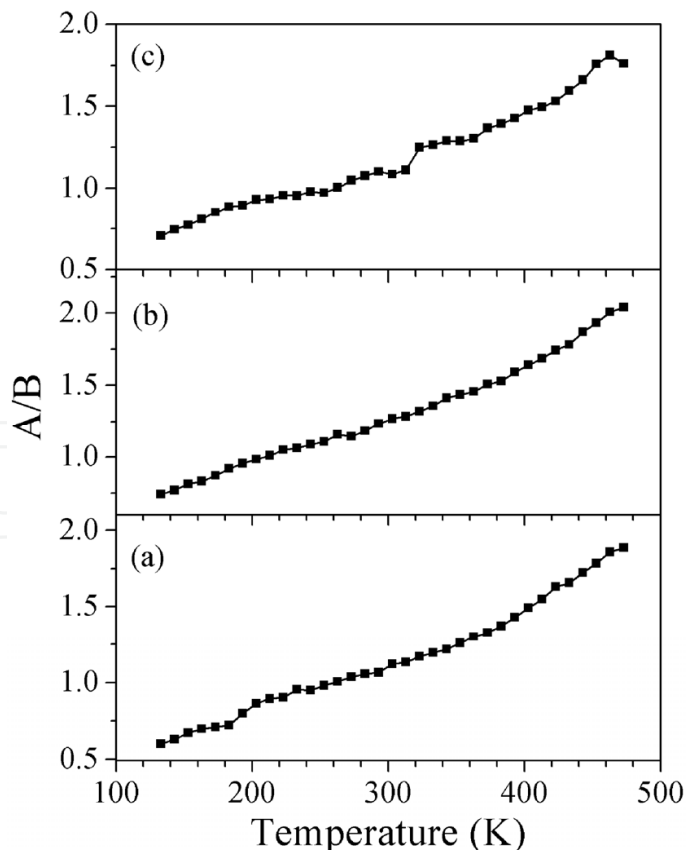

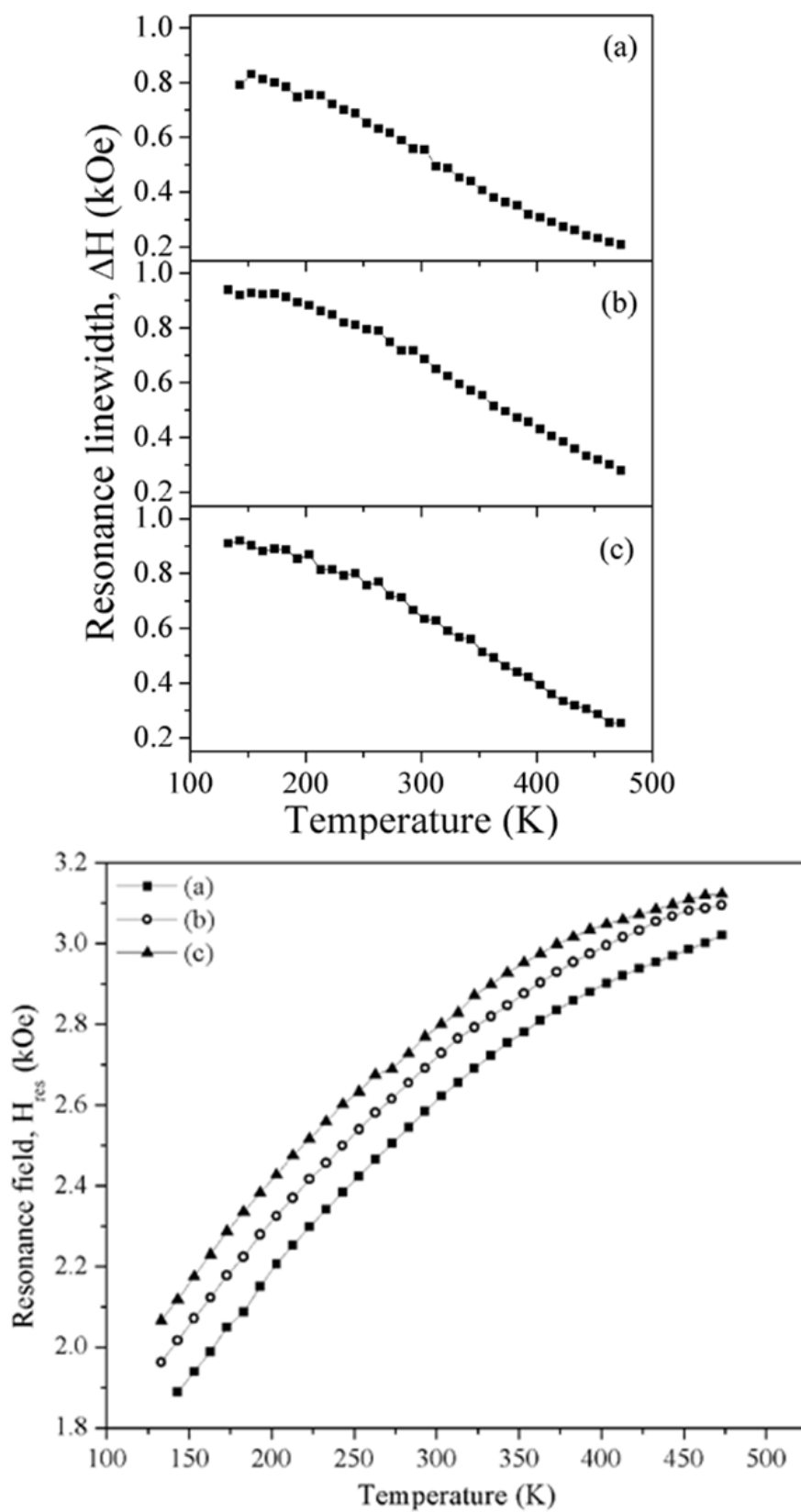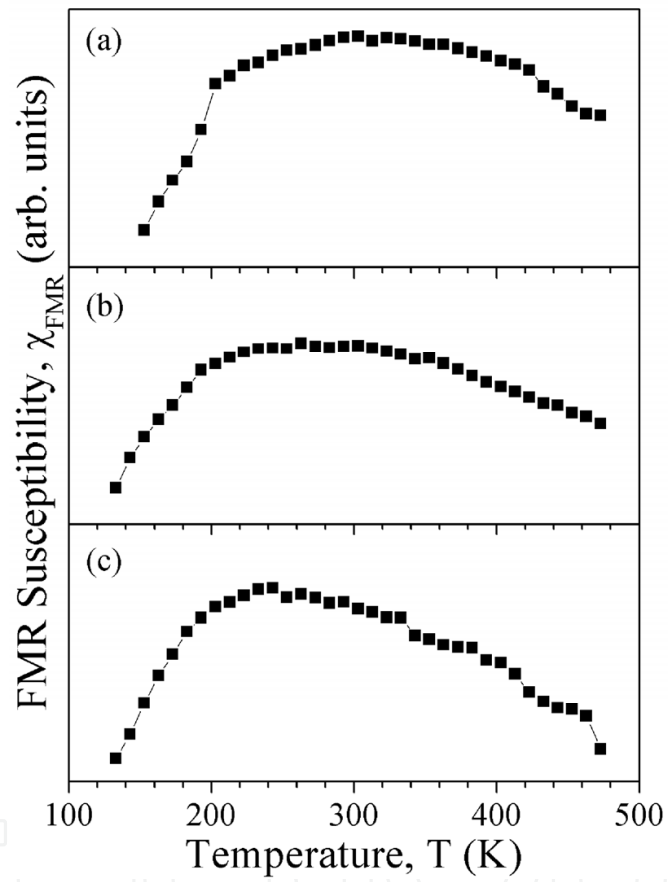**Figure 27.** Variation of A/B ratio of [SnO2 (x nm) CZF (83 nm)]5 with temperature for x = 46 (a), 115 (b) and 184 (c).

Figure 28. Variation of FMR resonance linewidth (top) and resonance field (bottom) with temperature of [SnO$_2$ (x nm) CZF(83 nm)]$_5$ for x = 46 (a), 115 (b) and 184 nm (c).

Figure 29. Variation of FMR susceptibility, χ_{FMR} with temperature of [SnO$_2$(x nm)CFZ(83 nm)]$_5$ ML for x = 46 (a), 115 (b) and 184 nm (c).
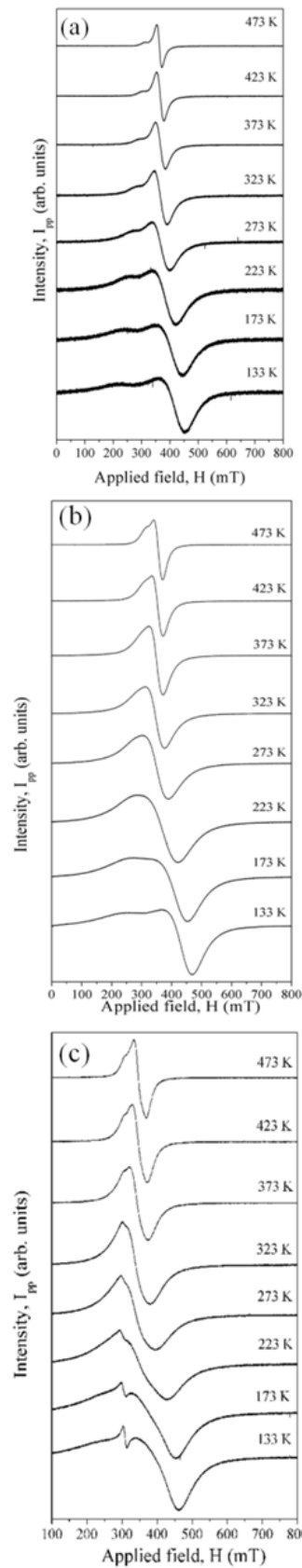
Figure 30. FMR spectra of [SnO$_2$ (x nm) CZF(83 nm)]$_5$ ML recorded at various temperatures in perpendicular configuration for x = 46 (a), 115 (b) and 184 (c).
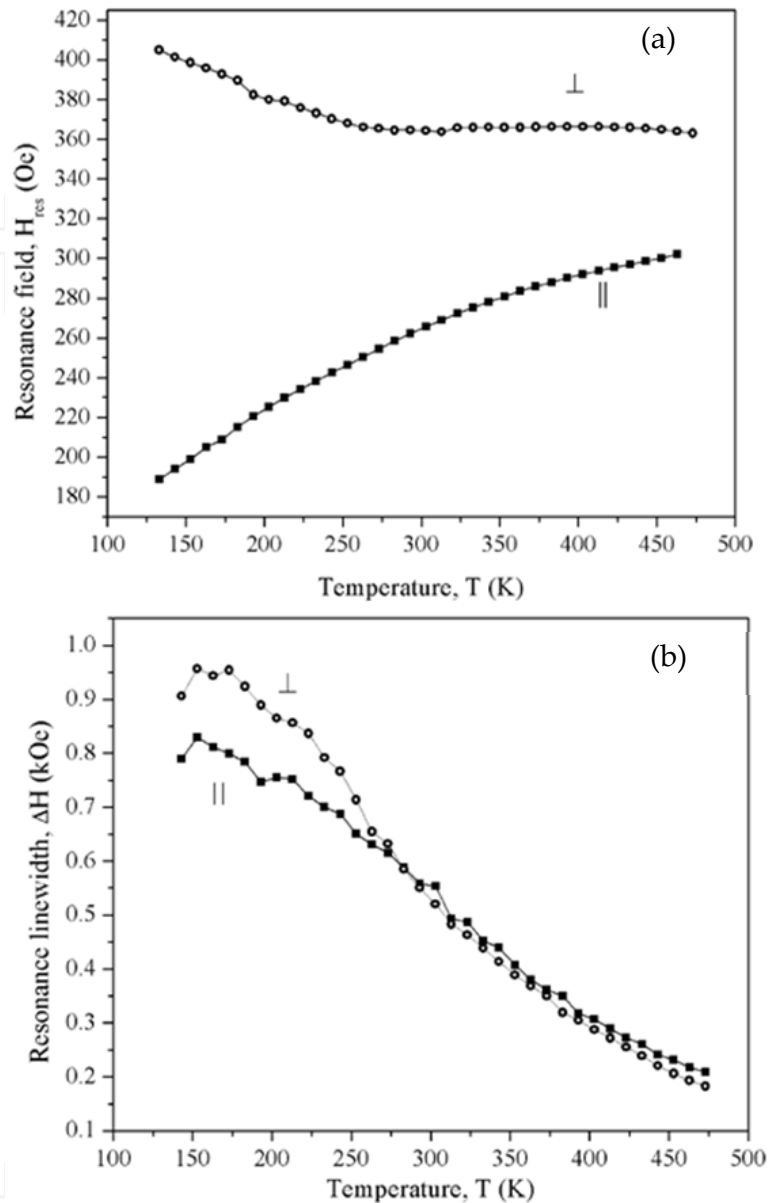
Figure 31. Variation of resonance field, H$_{res}$ (a) and resonance linewidth, ΔH (b) with temperature in parallel and perpendicular configurations for [SnO₂ (46 nm) CZF(83 nm)]₅ ML .

The effective magnetization is found to increase with decreasing temperature. Major contribution to the effective magnetization comes from the perpendicular anisotropy. This implies that as the temperature decreases the perpendicular anisotropy relaxes. χ$_{FMR}$ shows a different behavior as a function of temperature in the perpendicular configuration. Figure 32 is a representative plot of variation of χ$_{FMR}$ with temperature in parallel and perpendicular configuration. It increases continuously with decreasing temperature for all the ML in the perpendicular configuration.
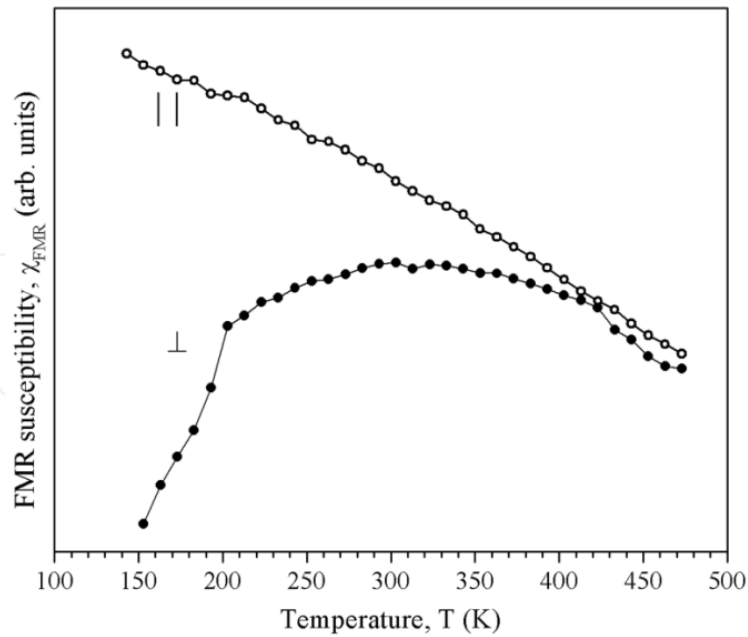
Figure 32. Representative plot showing variation of FMR susceptibility with temperature in parallel and perpendicular configurations for [SnO$_2$ (46 nm) CZF(83 nm)]$_5$ ML .

4. Conclusions

The temperature dependent ferromagnetic resonance (FMR) studies on [SnO$_2$/ Cu-Zn ferrite]$_n$ as function of magnetic layer and spacer layer thickness were carried out in the temperature range 100- 475 K. The study of temperature dependence of FMR lineshape, peak-to-peak linewidth, peak-to –peak line intensity and resonance field provide an insight into the interfacial effects. The inplane and out of plane FMR studies provide information about the magnetic anisotropies of the ML.

Author details

R.Singh and S.Saipriya
School of Physics, University of Hyderabad, Central University P.O., Hyderabad, India

5. References

[1] P. Bruno and C. Chappert, *Phys. Rev. Lett. B* 67 (1991) 1602

[2] D.M.Edwards, J.Mathon, R.B.Muniz, and M.S. Phan, *Phys. Rev. Lett.* 67 (1991) 493

[3] C.H.Marrows, Nathan Wiser, B. J. Hickey, T.P.A Hase and B.K. Tanner, *J. Phys.: Cond. Matter* 11 (1999) 81

[4] K. R. Nikolaev, A. Yu. Dobin, I. N. Krivorotov, W. K. Cooley, A. Bhattacharya, A. L. Kobrinskii, L. I. Glazman, R. M. Wentzovitch, E. Dan Dahlberg, and A. M. Goldman Phys. Rev. Lett. 85 (2000) 3728

[5]   D. M. Lind, S. D. Berry, G. Chern, H. Mathias, and L. R. Testardi, *Phys. Rev. B* 45 (1992) 1838.

[6]   M. A. James, F.C. Voogt, L. Niesen, O.C. Rogojanu and T. Hibma, *Surf. Sci.* 402 (1998) 332

[7]   P. J. Van der Zaag, R.M. Wolf, A.R. Ball, C. Bordel, L.F. Feiner and R. Jungblut, *J. Magn. Magn. Mater.* 148 (1995) 346

[8]   S. Saipriya, Joji Kurian and R. Singh, *IEEE Trans Mag.* 147 (2011) 10

[9]   S. Saipriya, Joji Kurian and R. Singh, AIP Conf. Proc. 1451 (2012) 67

[10] S. Saipriya and R. Singh, *Mater. Lett.* 71 (2012) 157

[11] S. Saipriya, Joji Kurian and R. Singh, J. Appl. Phys 111 (2012) 07C110

[12] M. Sultan and R. Singh, J. Appl. Phys. 107 (2010) 09A510

[13] S. Saipriya, M. Sultan and R. Singh, Physica B 406 (2011) 812

[14]   M. Sultan and R. Singh, *J. Phys. D: Appl. Phys.* 42 (2009) 115306

[15] G. S. Bales and A. Zangwill, J. Vac. Sci. Technol A 9 (1991) 145

[16] O. S. Josyulu and J. Shobanadri, *J. Mat. Sci.* 20 (1985) 2750

[17] Janhavi P. Joshi, Rajeev Gupta, A. K. Sood and S. V. Bhat, *Phys. Rev. B* 65 (2001) 024410

[18] Y. Gong, Z. Cevher, M. Ebrahim, J. Lou, C. Pettiford, N. X. Sun and Y. H. Ren, *J. Appl. Phys.* 106 (2009) 063916

[19] S. S. Yan, *Acta Metullurgica Sinica* 9 (1996) 283

[20] A. Ohtomo, D. A. Muller, J. L. Grazul and H. Y. Hwang, *Nature* 419 (2002) 378

[21] S.S. Kang, J.W. Feng, G.J. Jin, M. Lu, X.N. Xu, A. Hu, S.S. Jiang and H. Xia, *J. Magn. Magn. Mater.* 166 (1997) 277

[22] C. Kittel, *Phys. Rev.* 110 (1958) 1295

[23]   A. M. Portis, *Appl. Phys. Lett.* 2 (1963) 69

[24] S. J. Yuan, L. Wang, R. Shan and S.M. Zhou, *Appl. Phys. A* 79 (2004) 701

[25] R. D. McMichael, M. D. Stiles, P. J. Chen, and W. F. Egelhoff, Jr., *Phys. Rev. B* 58 (1998) 8605

[26] M. Sultan and R. Singh, J. Phys: Conf. Ser. 200, 072090 (2010).

[27] U. Gradmann and A Mueller, *Phys. Status. Solidi.* 27 (1968) 313

[28] M. T. Johnson, P. J. H. Bloemen, F. J. A. den Broeder and J. J. de Vriesy, *Rep. Prog. Phys.* 59 (1996) 1409

[29] J. H. Jung, S. H. Lim and S. R. Lee, *J. Appl. Phys.* 108 (2010) 113902

[30]   J. Pelzl et al, *J. Phys.: Condens. Matter* 15 (2003) S451

[31] M. C. Hickey and S. J. Moodera, *Phys. Rev. Lett.* 102 (2009) 137601

[32] Y. Tserkovnyak, Arne Brataas, Gerrit E. W. Bauer and Bertrand I. Halperin, *Rev. Mod. Phys.* 77 (2005) 1375

[33] G. Eliers, M. Lüttich and M. Münzenberg, *Phys. Rev. B.* 74 (2006) 054411

[34] R. Rai, K. Verma, S. Sharma, Swapna S. Nair, M. A. Valente, A. L. Kholkin and N. A. Sobolev, *J. Phys. Chem. Solids* 72 (2011) 862

[35] M. Marysko and J. Simsova, *Phys. Stat. Sol. A,* 33 (1976) K133-K136

[36] M. R. Diehl, J-Y Yu, J. R. Heath, G. A. Held, H. Doyle, S. Sun and C. B. Murray, *J. Phys. Chem. B* 105 (2001) 7913

[37] R. Topkaya, M. Erkovan, A. Öztürk, O. Öztürk, B. Aktaş and M. Özdemir, *J. Appl. Phys.*108 023910

[38] B. X. Gu and X. Wang, *Acta Metalurgica Sinica(English letters)*12 (1999) 181